Tittle Page

Underfilled peripheral foreland development in response to the Proto-Tethys Ocean closure in the North Qilian, NE Tibet Plateau

Jiaopeng Sun[a, b], Yunpeng Dong[a, c], Qiang Chen[d], Lei Yang[a], Wenhou Li[a], Qian Zhang[a], Dongdong Zhang[a]

[a] *State Key Laboratory of Continental Dynamics, Department of Geology, Northwest University, Northern Taibai Str.229, Xi'an 710069, China*

[b] *State Key Laboratory of Petroleum Resources and Prospecting, China University of Petroleum, FuxueRoad 18, Changping District, Beijing 102249, China*

[c] *Department of Earth Sciences, Western University, 1151 Richmond Street N. London, Ontario, N6A 3K7 Canada*

[d] *School of Earth Science and Resources, Chang'an University, Middle-section of Nan'er Huan Road, Xi'an 710054, China*

Corresponding author:

Jiaopeng Sun: E-mail address: sunjiaopeng@nwu.edu.cn;

Yunpeng Dong: E-mail address: dongyp@nwu.edu.cn.

Running Title: Late Ordovician underfilled peripheral foreland in the North Qilian

Key Points:

1. An underfilled peripheral foreland was formed in the western North China Block at ca. 453 Ma.
2. The initial closure of the eastern North Qilian Ocean was synchronous along-strike at ca. 453 Ma.
3. The accretion of the Central Qilian arc terrane onto the western North China Block began at ca. 453 Ma.

Abstract

The North Qilian Ocean (NQO) was the northernmost branch of the Proto-Tethys separating the Central Qilian Terrane (CQT) from the North China Block (NCB) since the Neoproterozoic Rodinia breakup. An enhanced knowledge on its evolutionary history would greatly improve our understanding on the tectonics of the Proto-Tethys and the assembly of the East Asia. However, the timing of the NQO closure onset remains unsolved with assumptions ranging from the end-Ordovician to the Devonian. To address this issue, integrated studies of stratigraphy, petrology and geochronology were conducted on the Ordovician strata in the SWNCB and the eastern North Qilian Accretionary Belt (ENQAB). Stratigraphic and paleontologic syntheses demonstrate that the pre-Katian strata in the SWNCB are shallow-marine deposits containing abundant benthonic faunas, while the Katian successions atop an unconformity are dominated by deep-water calcareous debrites and siliciclastic turbidites with the dominance of planktonic graptolites. Provenance analysis reveals an evolving source from the NCB basement to the CQT orogen since the Katian. The pre-Katian quartz arenites in the SWNCB contain zircons of ca. 1600–2800 Ma significantly older than their depositional timing, in contrast, the Katian turbidites in the SWNCB and the ENQAB display similar age patterns dominated by ca. 450–900 Ma ages. These clues imply a noteworthy basin-filling shift from passive margin to underfilled peripheral foreland separated by a forebulge unconformity at the Sandbian/Katian boundary. The first arrival of CQT-originated detritus onto the SWNCB at ca. 453 Ma is the oldest stratigraphic constraint for the initial elimination of the northern Proto-Tethys.

Key Words: Ocean closure; Peripheral foreland; Katian; North Qilian Ocean; North China Block.

1. Introduction

The Central China Orogenic System is a giant orogenic collage suturing the northern and southern China blocks (Figure 01a). It has been established to represent the relic of the northern Proto-Tethys and Paleo-Tethys (Metcalfe, 2013, 2021; Liu et al., 2005, 2015; Huang et al., 2018), making it crucial to understand geologic processes from the Rodinia break-up, via Gondwana assemblage, to Pangea assembly, which finally resulted in the amalgamation of the East Asian continent (Zuza & Yin, 2017; Domeier, 2018; Zhao et al., 2018; Metcalfe, 2021).

The Qilian Orogen at the central portion of the Central China Orogenic System occupies a key position as the northernmost tectonic collage of the Proto-Tethyan realm (Xiao *et al.*, 1978, 1986, 2009; Chang *et al.*, 1986; Bian *et al.*, 2001; Pan *et al.*, 2004, 2012; Xu *et al.*, 2013a; Zhang *et al.*, 2015a, 2019b; Li et al., 2017, 2018a; Dong et al., 2018a, b). It has become the focus of extensive research for decades. Multidisciplinary approaches have contributed to a better understanding on its tectonic architecture, complicated accretionary-collisional processes and subsequent intracontinental orogenesis (Xiao *et al.*, 1978, 2009; Yin & Harrison 2000; Gehrels *et al.*, 2003a, b; Xia *et al.*, 2003, 2016; Song *et al.*, 2006, 2007, 2013, 2017; Zhang et al., 2007, 2018; Yin et al., 2008). Nonetheless, there is still no consensus on the timing of the North Qilian Ocean (NQO) closure onset, e.g., the oceanic subduction termination, with diverse presumptions varying in age from the end-Ordovician to the Devonian (Yin & Harrison, 2000; Xiao et al., 2009; Xu *et al.*, 2010a, b, 2013b; Yan *et al.*, 2010; Gehrels *et al.*, 2011; Song *et al.*, 2013; Yuan & Yang, 2015; Zuza *et al.*, 2018). This unsolved tectonic issue has greatly hampered our knowledge on the convergent processes of the NQO and the geologic evolution of the Proto-Tethys Ocean.

Sedimentary-related records are sensitive to paleotectonic and paleogeographic interrelationships, playing an increasingly important role to test alternate paleogeographic and paleotectonic reconstructions in addition to known magmatic and metamorphic approaches (Dickinson & Suczek., 1979; Du *et al.*, 2003, 2009; Cawood *et al.*, 2012; Sun & Dong, 2020a). At the initial stage of arc-continent collision, closure of the intervening ocean may bring the edge of passive margin to collide with the arc terrane, generating an underfilled foreland along the suture zone (Sinclair et al., 1997; Aitchison et al., 2000; DeCelles *et al.*, 2014). Rock masses transported from the obducting orogenic highland to foreland at the low relief on the subducting plate preserve valuable clues to limit the time when the two blocks commenced to be juxtaposed (Dickinson, 1985; Hu et al., 2012, 2015, 2016; An et al., 2021). In the light of this simple

principle, identifying the oldest siliciclastic sedimentary rocks upon the western end of the SWNCB that contain detritus derived from the CQT arc will yield a straightforward and robust constraint on the timing of the ENQO closure onset, and by reference the resulted accretion of the CQT onto the SWNCB.

In the eastern North Qilian Accretionary Belt (ENQAB) and the SWNCB, relatively continuous and biostratigraphically well-constrained Ordovician successions are preserved around the North Qilian Suture. These pivotal stratigraphic imprints provide a unique window to constrain tectonic processes of the shrinking and closure of the ENQO. In this study, we integrate stratigraphy and paleontology with detrital zircon geochronology to demonstrate a Katian tectonic transition into underfilled foreland, witnessed by shift of paleogeography and source-to-sink relation in the ENQAB and the SWNCB. These new insights in basin-filling conversion allow us to propose a direct constraint on the timing of the collision onset between the CQT and the SWNCB, which will further shed light on subsequent studies concerning the Qilian Orogen.

2. Tectonic outline of the Qilian Orogen and the SWNCB

The Central China Orogenic System, striking in a NWW-SEE trend, stretches across the central China from the Kunlun-Qaidam-Qilian orogenic collage in the west to the Qinling-Dabie-Sulu orogen in the east (Figure 01a; Xiao et al., 2002a, b, 2005; Huang et al., 2018; Zhao et al., 2018; Sun et al., 2019, 2020; Zhao et al., 2020). The Early Paleozoic Qilian Orogen at the northern margin of the Tibetan Plateau occupies a conjunction among the SWNCB to the east, the Tarim Block to the west, and the Olongbuluke Terrane to the south (Figure 01b). It is truncated and sinistrally offset for ~400 km by the Altyn Tagh Fault that delineates its western border with the Tarim Block (Zhang et al., 2007, 2018; Song et al., 2013, 2019a; Qian et al., 2021). On the other side, it is continuous eastward to the North Qinling Orogen (Dong et al., 2011, 2021; Yan et al., 2006, 2014, 2019a; Zuza & Yin, 2017; Sun & Dong, 2020b).

The northern border fault of the Qilian Orogen dips southwards (Figure 01c) and extends eastwards from Longshoushan, Chahan, via Qintongxia, to Guyuan, namely the Longshoushan Fault (Figure 01b; Dong et al., 2021). Lying to its north is the SWNCB that incorporates the Alxa Terrane in the west and the Ordos Basin (Block) in the east (Figure 01b; Zhang & Gong, 2018; Sun & Dong, 2019 a, b). Much of the SWNCB is floored by an Archean to Paleoproterozoic basement that was finally crystallized at ca. 1.8 Ga

(Zhao et al., 2002, 2005, 2012; Zhao & Cawood, 2012; Zhang et al., 2013, 2015b; Wu et al., 2021a) prior to the accumulation of non-metamorphosed sedimentary cover from the Mesoproterozoic to present (Figure 01d; Chen, 2011; Sun & Dong, 2019c). Some Meso- and Neoproterozoic terranes in the western Alxa Terrane, which were accreted to the SWNCB in the Paleozoic (Sun & Dong, 2020a), complicate its tectonic composition and geologic history.

The Qilian Orogen is a wide orogenic collage that can be further divided into three sub-parallel units with distinct litho-tectonic fluctuation and resulted tectono-lithostratigraphy, including, from north to south, the NQAB, the CQT, and the South Qilian Accretionary Belt (Xiao et al., 2009; Li et al., 2017; Song et al., 2017; Sun et al., 2019, 2020; Dong et al., 2021).

In contrast to the SWNCB, the NQAB was active from the Neoproterozoic to the Paleozoic (Figure 01d), characterized by the occurrence of the end-Neoproterozoic to the Early Paleozoic accretionary mélange-ophiolite complexes (Song, 1997; Qian et al., 1998, 2001; Zhang et al., 2001, 2007; Xia & Song, 2010; Fu et al., 2019a, 2020a, 2021a), subduction-collision induced volcanic and plutonic rocks (Song et al., 2013), high-pressure metamorphic rocks (Zhang et al., 2001, 2007; Song et al., 2006, 2007; Fu et al., 2020b), as well as the Ordovician to the Devonian flysch and molasse formations (Yan et al., 2007, 2010; Yang et al., 2009; Xu et al., 2010a, 2013a). The NQAB has been interpreted to be a typical oceanic suture zone as a product of the end-Neoproterozoic to the mid-Paleozoic opening, spreading, south-dipping subduction, and ultimate termination of the NQO (Sobel & Arnaud, 1999; Geherels et al., 2003a, b). This ocean could be traceable eastwards with the Erlangping Ocean between the North Qinling Arc Terrane and the NCB (Dong et al., 2011, 2015, 2018b; Yan et al., 2016; Song et al., 2017).

The CQT is an early Paleozoic arc terrane underlain by an imbricated thrust belt of Precambrian crust that is composed mostly of 850–1000 Ma garnet-bearing granitic gneiss (Gehrels et al., 2003b; Tseng et al., 2006, 2009; Tung et al., 2007a, 2013) and paragneiss with detrital zircon ages older than 880 Ma (Tung et al. 2007b). Minor amounts of Paleoproterozoic migmatitic granites dated at ca. 1800 Ma and ca. 2500 Ma (Wang & Chen, 1987; Gehrels et al., 2003a) as well as the Meso- to Neoproterozoic cratonal and/or passive marginal strata also exist (Gehrels et al., 2003a; Wu et al., 2016; Zuza et al., 2018). The crystalline basement of the CQT has been intensively reworked by ca. 440–520 Ma arc magmatic activity and ca. 400–435 Ma collisional to post-orogenic magmatism (Gehrels et al., 2003b; Song et al., 2013, 2019a; Tung et al., 2016; Fu et al., 2019b, c) as a consequence of closure of oceanic basins to its southern and northern sides. The CQT has been hypothetically proposed to be comparable with the North Qinling Arc Terrane, given

the similarity of the Precambrian basement and two episodes of orogeny during the Grenville and Caledonian age (Li et al., 2017; Zhao et al., 2020).

The South Qilian Ophiolite-Accretionary Belt is a belt of subduction–accretion complexes (Pan et al., 2012; Yan et al., 2015, 2019b; Song et al., 2017; Fu et al., 2018; Yang et al., 2019). It is characterized by the exposure of the end-Neoproterozoic to the Early Paleozoic subduction-related volcano-sedimentary rocks with several accreted terranes preserved in the east (Yan et al., 2015; Song et al., 2017). Dismembered ophiolites with formation ages of the end-Neoproterozoic to the Ordovician discontinuously outcrop along and in fault contact with the southern rim of the CQT, including, from west to east, the Dadaoerji, Muli, Gangcha, and Lajishan ophiolites generated mostly in the supra subduction zone location above a north-dipping oceanic crust (Fu et al., 2018; Yan et al., 2019a, b; Yang et al., 2019). Lying to the south of these arc–ophiolite complexes is a widespread belt of, tightly folded, cleaved, siliciclastic and volcaniclastic turbidites (Xiao et al., 2009), intruded by the pervasive mid-Paleozoic plutons (Dong et al., 2021). These deep-water sediments have been mapped as the Ordovician to the Silurian strata, while several weighted mean ages of ~720–740 Ma have been obtained from volcanic rocks (Yan et al., 2021), hinting at a much earlier depositional onset and a likely longer accretionary history. This belt is traceable further east to the Shangdan Suture in the east Qinling Orogen (Yan et al., 2015; Dong & Santosh, 2016; Song et al., 2017; Li et al., 2018b; Zhao et al., 2020).

In this study, we mainly focus on an area at the conjunction of the southwestern Ordos Basin, ENQAB and CQT, stretching across the tectonic limit between the SWNCB and the eastern Qilian Orogen (e.g., the eastern segment of the Longshoushan Fault: Figure 01b).

3. Ordovician stratigraphy and sedimentology of the SWNCB

3.1 Stratigraphic units and depositional timing

Nine stratigraphic columns of outcrops and drill cores, distributed along-strike to the eastern side of the LSF (Figure 01b), were synthesized to show Ordovician stratigraphy and sedimentology of the southernmost NCB (Figures 02&03). Chronostratigraphic estimates of each stratigraphic unit and lateral correlation among different columns employ an updated chronostratigraphic proposal (Figure 02) on basis of high-precision conodont and radiolarian biostratigraphy and zircon U-Pb dating (Jing *et al.*, 2015, 2020; Zhen et al., 2016; Fan et al., 2020; Zhang et al., 2019a; Perera & Aitchison, 2021). Numerical ages noted in

Figure 02 are according to the timescale of Cohen et al., (2013). Five stratigraphic units with distinct lithological assemblages were termed to as the Sandaokan, Zhuozishan, Kelimoli, Wulalke and Lashizhong formations, in ascending order (Figure 02). The Ordovician stratigraphy in the SWNCB is shaped by two stratigraphic breaks, an earlier one separating the Middle Ordovician successions from the underlying Cambrian strata and a younger one at the Sandbian-Katian boundary. This work focuses on the upper Zhuozishan, Kelimoli, Wulalike, and Lashizhong formations deposited in the Late Ordovician (Figure 03).

Stratigraphic age of the Kelimoli Formation has been deduced to be the end-Darriwilian on account of conodont biostratigraphy (Jing et al., 2015). However, Wang et al. (2013, 2016a) argued that these conodont assemblages belong instead to the Sandbian or Katian, which is in excellent agreement with proposals of Perera and Aitchison (2021) that assigned a late Sandbian age for radiolarian faunas obtained from the lower section. Seven robust weighted mean ages (2σ) of 454.9±3.4 Ma to 449.9±1.7 Ma (Figure 02) have been obtained for tuff layers in the Kelimoli and Wulalke formations, identical within error to late Sandbian to Katian age indicated by biostratigraphy. These insights constrain deposition onset to the earliest Katian (ca. 453 Ma). The highest level of the Katian strata in the SWNCB have been suggested to be ca. 448 Ma (Chen et al., 2013). Thus, the Kelimoli, Wulalike, and Lashizhong formations can be reinterpreted to be the Katian with a short period of ca. 453–448 Ma. Meanwhile, deposition of the underlying Zhuozishan Formation may sustain to the Sandbian from the late Darriwilian (Zhen et al., 2016; Zhang et al., 2019a).

3.2 Pre-Katian shallow carbonate shelf facies (Sandaokan and Zhuozishan formations)

Stratigraphic contact below the Darriwilian Sandaokan Formation is a craton-wide unconformity overlying layers of diverse ages from the Cambrian to the Early Ordovician (Myrow et al., 2015; Zhen et al., 2016). A set of terrestrial sediments composed of gravel-bearing quartz arenites and carbonate clasts constitute the base of the Sandaokan Formation in the Zhuozishan, grading southward to thick dolostone with a small amount of sand-sized quartz grains in the Qinlongshan (Yang et al., 2011). The Sandaokan Formation consists of thick beds of dolostone interbedded with limestone and quartz sandstone (Li et al., 2021). Carbonate beds are mostly bioturbated and contain abundant benthic gastropods, brachiopods, and cephalopods (Fei et al., 2004). This mixed carbonate-siliciclastic sequence represents neritic deposition in a relatively shoreward inner shelf portion (Mount, 1984; Fei et al., 2004; Varejão et al., 2021). Limestone, mostly massive bedded bioclastic grainstone and packstone (Figures 04a, b), dominates the lithology of the

Zhuozishan Formation (Li et al., 2012; 2020) that conformably overlies the Sandaokan Formation. Patch reefs and mounds (Figure 04c) also present (Zhao et al., 2014). This lithofacies association and the enrichment of benthic faunas (Jing et al., 2015) imply deposition in a seaward shallow shelf far away from the terrigenous influx. Collectively, the Darriwilian to Sandbian sequence represents a nearly uninterrupted sedimentation in shallow-water carbonate shelf environments and records an overall transgression from shoreline and nearshore settings to more offshore environments (Feng et al., 1998; Myrow et al., 2015; Sun & Dong, 2020a).

3.3 Katian deep-water assemblages (Kelimoli, Wulalike and Lashizhong formations)

The Zhuozishan Formation is capped by a disconformity (Guo et al., 2012), where the major lithology changes abruptly from thick stack of bioclastic limestone to rhythmic thin- to medium-bedded lime mudstone (Figure 04d) with thin interbeds of shale and calciturbidite, and then grade upwards into multi-episodic slumps (Chen, 2011; Ma et al., 2013) slides and debrites (Figure 04e). Surfaces of limestone beds are planar to nodular with sets of beds mappable over wide areas (Figure 04f). The uneven fabric and the occurrence of subaqueous mass-transport deposits indicate deep-water gravitational settling of calcareous oozes (Wang et al., 2021a) that were winnowed from adjacent shallow platforms to an unstable slope (Sun & Dong, 2020b). This insight is supported by paleontological observations (Jing et al., 2015) that noted the dominance of radiolarian faunas and planktonic graptolites (Fu et al., 1993). Volcanic interbeds are common in outcrops and have been identified in core drillings (e.g., Yutan 1; Kang, 2021). Lateral stratigraphic relation shows that the bathyal carbonate slope varied eastwards into shallow platform as exemplified by thick deposition of bioclastic limestone and dolomite around wells Lucan 1 (Figure 03) and Gutan 1 (Ma et al., 2013; Wu et al., 2018). The inferred westwards deepening topography is coherent with WNW-dipping palaeoslope based on measurements of slumped folds, imbricated thrust beds, imbricated breccia, and strike of channels (Li et al., 2021).

The Wulalike Formation underlying the Lashizhong Formation (Figure 05a) is dominated by pelagic black graptolite-bearing shale (Figure 05b; Li et al., 2012; Chen et al., 2020), thin beds of radiolarian chert and lime mudstone with interlayers of gravity flow deposits (Figure 05c). Breccias are mostly irregular and chaotic limestone gravels, the lithologies of which are consistent with rocks of the underlying Kelimoli Formation, although in a few cases mixed lithologies exists (Figure 05d). Beds of breccias generally show lenticular morphology with erosional bases and substantial variation in lateral thickness (Ma et al., 2013).

Faunas obtained from this unit comprise mixed shallow-water and in situ deep-water forms (Jing et al., 2015). The Wulalike Formation represents deposition in a slope-basin transition, where in-situ pelagic basin plain shales were deposited and were continually disturbed by the redeposition of carbonates that constructed submarine fans around the slope apron (Gao et al., 1995; Li et al., 2012).

The Lashizhong Formation is typical siliciclastic turbidites (Sun & Dong, 2020a) composed of alternating greenish-gray shale, sandstone and thin bedded argillaceous limestone (Figure 05e), from which *Nereites* ichnofacies representing deep-marine environment have been found (Fei, 2001). Mass movement deposits, such as slides and slumps (Figure 05f), are common. Coeval successions in the ENQAB, e.g., the Miboshan Group, are also siliciclastic turbidites (Figure 05g) reworked by gravity-induced mass transportation (Figure 05h). These siliciclastic flysches indicate accumulation in a politic abyssal plain punctuated by turbidity currents in front of subaqueous fans relatively far from the continental rise (Sun & Dong, 2020a).

4. Provenance data: sandstone petrology and detrital zircon U-Pb geochronology

Analytical methods of sandstone petrology and detrital zircon U-Pb geochronology, as well as reprehensive mircophotos for sandstone and cathodoluminescence (CL) images of analyzed zircons are listed in the **Appendix**.

3.1. Petrographic composition

The Cambrian Sample SYSX01 is quartz arenite; its petrology is similar with other Cambrian to Middle Ordovician samples obtained from the SWNCB. Principal grain types are dominated by monocrystalline quartz grains, with a few amounts of polycrystalline quartz grains. Framework grains are well rounded and moderately sorted, indicating high textural and compositional maturity.

In contrast, the Upper Ordovician samples from the SWNCB (e.g., the Lashizhong Formation) and the ENQAB (e.g., the Miboshan Formation) are generally subangular and poorly sorted, characteristic of low textural maturity. According to the petrologic classification proposed by Pettijohn (1975), these sandstones are mostly sublitharenite or subfeldspathic arenite (Figure 06a) with moderate compositional maturity. These sublitharenitic and subfeldspathic arenites are characterized by a variably ranging percentage of

monocrystalline quartz (27.1–76.1 %), feldspar (1.5–29.9 %) and lithic fragments (6.6–68.0 %). Except for the Shibangou section, samples from which comprise a large amount of limestone lithic fragments (12.7–55.3 %), samples from other sections are dominated by 44.8–76.1 % of monocrystalline quartz grains, and relatively lack lithic grains (2.6–18.9 %). Averaged modal composition values of Qt/F/L and Qm/F/Lt are 70.8/8.7/16.4 and 62.6/8.7/24.6, respectively, which both fall within the range of "continental block provenances" (Figure 06b) and "recycled orogeny provenances" (Figure 06c) on the tectonic discrimination diagrams of Dickinson (1985). In comparison, those for the Cambrian to Middle Ordovician all plot in the field of "craton interior sediments". This inference is coherent with result of the Qp/Lv/Ls diagram that depicts a mixed orogen source (Figure 06d).

3.2. LA-ICP–MS zircon U–Pb dating

Eight representative medium- to coarse-grained sandstone samples and one tuff sample were selected for zircon U–Pb dating by Laser ablation-inductively coupled plasma-mass spectrometry (LA-ICP-MS). Of these eight sandstone samples, one (Sample SYSX01) is from the Cambrian Xuzhuang Formation in the SWNCB, five samples are from the Upper Ordovician Lashizhong Formation in the SWNCB and two samples are from Upper Ordovician Miboshan Formation in the ENQAB. Approximate geologic locations and stratigraphic levels of these samples from this and published studies were shown on Figures 01b & 03, respectively. Detailed information on location and petrology of each sample is listed in the Appendix Part 2.

3.2.1. Cambrian quartz arenite

Zircons from the Cambrian Sample SYSX01 are well rounded and sorted with clear margin of abrasion. Diameters of unbroken grains range from 80 μm to 100 μm. On the CL image, majority of zircons show clear oscillatory zoning and nebulous internal structures, with a few grains being sector-zoned or structureless.

A total of 100 analyses on 100 grains produced 88 data with sufficient precision for geochronological interpretation (Figure 07a). The concordant ages are all Paleoproterozoic, falling in the span of ca. 1584 Ma to ca. 2826 Ma, and are grouped into two major clusters (Figure 07b). The early Paleoproterozoic cluster contains 37 ages and constitutes a narrow peak at ca. 2446 Ma. The late Paleoproterozoic population is composed of 32 data that define a wide peak at ca. 1801 Ma. A small number of ages occur at ca. 1970 Ma

to ca. 2187 Ma with two poorly defined peaks at ca. 2010 Ma.

3.2.2. Upper Ordovician turbidite

Zircons from the Upper Ordovician sandstones are mostly prismatic euhedral fragments, with some sub-rounded to rounded grains displaying abrasive shapes (Figures 07b, c, d, e, f, g & h). The lengths of unbroken grains vary variably from 60 μm to 180 μm with aspect ratios of 1:1 to 2:1. Most grains exhibit oscillatory zoning and nebulous internal structures in CL images, and a few grains show core-rim and plate structures. Most of them have Th/U values greater than 0.1, indicating an igneous origin (Belousova et al., 2002; Corfu, 2003). Minor amounts of grains display homogeneous or structureless structures with low Th/U ratios, likely suggesting a metamorphic origin.

Analyses on the Lashizhong Formation sandstone SMN01 from the Xishan section yielded 115 concordant results ranging in age from 489±10 Ma to 3215±35 Ma, and display age peaks at ca. 490 Ma, ca. 565 Ma, ca. 776 Ma, ca. 959 Ma, ca. 2463 Ma and ca. 2664 Ma (Figures 07c & d). Two major age populations display peaks at 959 Ma composed of 28 ages of 900–1018 Ma and 2463 Ma composed of 18 ages of 2433 Ma–2798 Ma. Six ages of 1603–1717 Ma define a subordinate peak at 1633 Ma.

A total of 113 concordant ages obtained from the Lashizhong Formation sandstone SXG03 from the Xianggen section span from 514±10 Ma to 3500±31 Ma (Figures 07e & f). Three oldest zircons have ages of 3046±35 Ma, 3412±31 Ma and 3500±31 Ma. The largest age clusters include 27 ages between 961 Ma and 1053 Ma with a single peak at 1024 Ma. Secondary clusters peaking at 1748 Ma and 2462 Ma also present.

A total of 120 analyses on zircons of the Lashizhong Formation sandstone SGK03 generated 109 concordant data. Its age spectrum spans from 451±11 Ma to 3542±32 Ma (Figures 07g & h). This sample is characterized by the early Paleozoic results, which comprise 56 data of 451±11–470±11 Ma and define a prominent peak at ca. 466 Ma. A few ages make up subsidiary peaks at 956 Ma (13 ages between 888 Ma and 976 Ma) and 2440 Ma (5 ages between 2363 Ma and 2485 Ma).

Up to 120 datings on the Lashizhong Formation sandstone SHX04 collected from the Shibangou section yielded 108 reliable ages (Figures 07i & j). The notable age cluster occurs at ca. 995 Ma, with secondary ages peaking at ca. 1607 Ma and ca. 2482 Ma.

A total of 120 analyses on the Lashizhong Formation sandstone SHX06 from the Shibangou section generated 110 ages with less than 10% discordance (Figures 08a & b). These ages fall in the range from

311 533 Ma to 3532 Ma. Nineteen ages of 2360–2563 Ma, twenty-two ages of ca. 900–1022 Ma and thirteen
312 ages of ca. 1522–1675 Ma define 3 peaks at 2497 Ma, 969 Ma and 1603 Ma.
313 A total of 100 analyses on 100 zircons from the Miboshan Formation sandstone SJSP01 yielded 99
314 isotopic data of acceptable discordance and precision, ranging in ages from 448±9 Ma to 3483±31 Ma
315 (Figures 08c & d). One youngest zircon yields a Late Ordovician age of 448±9 Ma. Major age groups occur
316 at 656 Ma to 2728 Ma and define a single age cluster of 900–1100 Ma with a highest age peak at 964 Ma.
317 Secondary age populations define some subdominant peaks at ca. 1580 Ma, ca. 1834 Ma, and ca. 2440 Ma.
318 Two scatted late Neoproterozoic ages are 622±11 Ma and 624±6 Ma.
319 Of the up to 100 analyses on the Miboshan Formation sandstone SWRO01, 98 analyses plot on or near
320 the concordia and yield ages with less than 10% discordance (Figures 08e & f). The concordant ages vary
321 from 447±9 Ma to 2565±36 Ma. Thirteen Early Paleozoic ages were detected; the youngest 8 ages are
322 clustered in the range of 447±9 Ma to 461±9 Ma and yield a weighted average age of 453±3 Ma (Figure
323 08e). The majority of ages fall in the span of ca. 1300–1700 Ma, with three unobvious peaks at ca. 1418, ca.
324 1600 and ca. 1736 Ma. Some Neoproterozoic ages define two secondary peaks at ca. 777 Ma and ca. 901
325 Ma.
326
327 **3.2.3. Upper Ordovician tuff**
328 A total of 48 analyses on the volcanic sample SJT-05 from a tuffaceous layer of the lower Lashizhong
329 Formation at the Pingliang section generated 41 concordant ages between 444±10 Ma and 456±10 Ma,
330 which define a weighted average age of 452±3 Ma with mean squared weighted deviation (MSWD) =
331 0.071 (Figures 08g & h).
332

333 ## 5. Discussion

334 ### 5.1. The NCB-Qilian provenance reversal at the Katian

335 Paleogeographic reconstructions reveal a reverse of sediment supply in the SWNCB from northeast to
336 southwest (present coordinate) at the Katian. Paleocurrent directions, obtained from orientated fossils in the
337 end-Darriwilian Sandaokan Formation, indicate the Middle Ordovician sediment transport from the
338 northeast (Fei et al., 2004), consistent with stratigraphic correlation that shows southward-decreasing
339 terrestrial influx from tens of meters thick quartz sandstone to pure carbonate (Sun & Dong, 2020a). In

contrast, paleocurrent directions, measured from the Katian Lashizhong Formation, direct northeastwards to eastwards (Figure 03; Gao et al., 1995), inferring northeastward sediment dispersal. Facies distribution also displays decreasing siliciclastic influx towards the northeast, until termination in the well Lucan 1 where turbidites are absolutely absent (Figure 03). Triangular diagrams also highlight a sharp compositional change from the end-Darriwilian pure quartz arenites derived from cratonic interiors to the Katian subfeldspathic/sublithic arenites sourced from mixed orogen sources (Figure 06).

This evolving provenance is also supported by the changing detrital zircon U-Pb age spectra. Age patterns of the Middle Ordovician quartz arenites of the SWNCB compare well with those of the underlying Mesoproterozoic to Cambrian samples (Figure 09a), which comprise zircons without ages younger than Paleoproterozoic. However, age relations for turbidites from the Late Ordovician Lashizhong Formation (Figure 09b) are very similar to those of time-equivalent Miboshan Formation in the ENQAB (Figure 09c), comprising mostly post-Mesoproterozoic ages with a strong peak at ca. 950 Ma or ca. 460 Ma, notably close to their depositional timing.

Cratonization of the NCB was terminated by the amalgamation of the Yinshan (Alxa) and Ordos Blocks along the Khondalite Belt at ca. 1.92 Ga (Zhao et al., 2005; Zhao et al., 2012; Wan et al., 2013; Zuza & Yin, 2017). Its Archean and Paleoproterozoic crystalline basement (with predominately ca. 2.5 and 1.95–1.80 Ga ages; Sun & Dong, 2019c, Liu et al., 2021) was subsequently stable and capped by shallow marine deposits accumulated in rift to passive margin settings from the Mesoproterozoic to the Paleozoic age (Gehrels et al., 2011; Zhao & Cawood, 2012; Dong & Santosh, 2016). The post-Paleoproterozoic magmatic activities occur rarely and are even absent in the Paleozoic, except for a few ca. 900 Ma-aged mafic dikes (Peng et al., 2011; Peng, 2015). In contrast, crustal evolution of the CQT was constructed by two major episodes of pervasive granitic pluton emplacements at the Neoproterozoic and the Paleozoic (Gehrels et al., 2003b; Yong et al., 2008; Xia et al., 2012; Song et al., 2013; Yu et al., 2013, 2021). Thus, the presence and/or absence of ubiquitous magmatic flare-ups of ca. 900 Ma and ca. 460 Ma makes us easily distinguishing sources from each unit.

All NCB-originated sandstones yield two age peaks at ca. 1850 and ca. 2450 Ma (Figure 09a), characteristic of those identified from the NCB basement (Figure 10a; Darby & Gehrels, 2006; Sun & Dong, 2019c). Therefore, we attribute the provenance of the Pre-Katian strata to the erosion of the SWNCB basement to the northeast and possible recycling of older covers sourced from it (Sun & Dong, 2020a). In the northeastern Ordos Basin, a topographic high termed as the Yimeng highland (Figure 01b) existed in

the Ordovician (Li et al., 2012, 2020), where ca. 2500 Ma supracrustal rocks and ca. 2000–2200 Ma granitic rocks as the basement of the Yinshan and Ordos Blocks were exposed then (Zhao et al., 2005, 2012; Jian et al., 2012; Dong et al., 2013; Liu et al., 2018a, b, 2020, 2021). In addition, ca. 1850–1950 Ma khondalite series that recorded continent–continent collision between the Yinshan and Ordos Blocks were exposed in the Khondalite Belt (Zhao et al., 2002, 2012; Yin et al., 2009, 2011; Li et al., 2011).

As discussed above, the Neoproterozoic to the Paleozoic tectonic activities are not substantial in the SWNCB, whereas age distributions of the Late Ordovician turbidites from the SWNCB and the ENQAB are all characterized by the dominance of age populations of both stages (Figures 09b & c). The strong similarity of age patterns between the CQT with the Late Ordovician Miboshan and Lashizhong formations (Figures 10b & c) allows us to invoke the CQT as a more likely source. The basement of the CQT is mostly composed of orthogenesis with ages of ca. 800–1000 Ma (Guo et al., 1999; Tung et al., 2007a; Yan et al., 2015; Wu et al., 2017b), responsible for the largest ca. 900 Ma cluster in most samples. The dominance of ca. 450–520 Ma grains in few samples (e.g., samples SGK03 and LSY) are attributed to penecontemporaneous magmatic activities in the CQT (Song et al., 2013; Li et al., 2017; Fu et al., 2021b). In addition, some scholars preferred to regard the presence of ca. 1800 and ca. 2500 Ma detritus as a signal of sedimentary supply from the NCB (Xu et al., 2013a). However, in this period, carbonate sedimentation existed throughout the Ordos Basin; the absence of carbonate lithic fragments excludes the possibility of sediment input from the NCB. Meanwhile, recent studies have demonstrated tectonothermal events of such episodes in the CQT and the Olongbuluke Terrane (Sun et al., 2019) to its south (see its location in Figure 01c). Older basement paragneiss in the CQT also contains detrital zircons with ages between ca. 1800 and ca. 2500 Ma (Gehrels et al., 2003b; Tung et al., 2007a; Yan et al., 2015; Liu et al., 2018b). Therefore, the appearance of zircons with ages of ca. 1800 and ca. 2500 Ma are not age-specific, making it unnecessary to require a contribution from the NCB. Moreover, our data do not rule out the possibility of a more proximal source from the older forearc successions in the ENQAB based upon the presence of low-grade metasedimentary fragments and the similarity of age profiles.

5.2. Subduction polarity and ca. 453 Ma synchronous closure of the North Qilian Ocean

5.2.1. ca. 453 Ma initial closure of the ENQO and the CQT-WNCB collision onset

One unresolved primary issue regarding the North Qilian Orogen is the timing of the initial elimination of the NQO and resultant accretion of the CQT onto the SWNCB (Fu et al., 2018; Zuza et al.,

2018), with hypotheses of the Ordovician/Silurian boundary (Yin & Harrison, 2000; Xia et al., 2003; Song et al., 2013), the middle Silurian (Sobel & Arnaud, 1999; Gehrels et al., 2003a, b; Fu et al., 2018, 2021a), and the Devonian (Xiao et al., 2009; Yuan & Yang, 2015). The timing of collision onset is most aptly defined as the moment when the distal edge of the passive margin came into physical contact with and subducted beneath the arc system (DeCelles et al., 2014; Hu et al., 2015, 2016; An et al., 2021). Instantly, detrital aprons from the opposite landmasses will comingle at abyssal depths on shelf or slope of the former passive continental margin (DeCelles et al., 2014). Hence, dating siliciclastic sedimentary rocks that contain detritus derived from the CQT and rested stratigraphically upon the westernmost NCB will provide a most direct and robust constraint (Garzanti et al., 1987) on the timing of the initial ENQO closure.

The Mesoproterozoic to the Middle Ordovician deposition with sources from the SWNCB basement requires the study area to be a coherent part of the SWNCB throughout that period, and indicates that the Lashizhong turbidites were in-situ deposited upon the SWNCB continental lithosphere. The overall age spectrum of the Katian Lashizhong turbidites is very similar with a strong degree of overlap to those of time-equivalent successions in the ENQAB (Figures 09b, c), suggesting that they shared a common provenance and their depositional sites were linked. Therefore, we can confirm that no matter how many branches once existed in the ENQO, all these oceanic basins should have been terminated to allow the SWNCB receiving the CQT-derived detritus at no younger than ca. 448 Ma. Given that the study area situates at the westernmost flank of the NCB, rather proximal to the suture zone (Figure 01b), this time estimate may be the oldest archive of the CQT-WNCB collision onset. It is clear that a lag time for the progressive progradation of turbidite to the SWNCB exists, and the time when passive continental lithosphere started to subside intensively is closer to the initial timing of arc-continent collision (DeCelles et al., 2014). Thus, another consideration is the unconformity directly capped by carbonate slope successions of the Kelimoli Formation, given that this stratigraphic break can be inferred to represent the forebulge uplift during the flexural passage over the SWNCB (see discussion below), which occurred slightly older at ca. 453 Ma.

Such an age bracket is fully compatible in error with several lines of evidences of collision induced clues retrieved from the Qilian Orogen, including (1) the age of the youngest Laohushan ophiolite (448±5 Ma; Song et al., 2013), (2) the latest arc-related volcanism (446±3 Ma; Wang et al., 2005) followed by syn-collision granitic plutonism of ca. 445 Ma (Li et al., 2017; Dong et al., 2021; Wu et al., 2021a), (3) the youngest major pulse of plutonism of ca. 445 Ma (Wu et al., 2016), (4) the youngest matrix monazite ages

(ca. 450–420 Ma; Zuza et al., 2018), (5) the cessation of ductile shearing by ca. 445 Ma (Zuza et al., 2018), (6) the ca. 454–442 Ma $^{39}Ar/^{40}Ar$ mica cooling ages (Liu et al., 2006), (7) the high-grade blueschist metamorphism of 446–454 Ma (Liou et al. 1989; Liu et al. 2006), and (8) the Silurian foreland basin deposition (Dong et al., 2021). Collectively, we argue for a CQT-WNCB collision onset at the Katian (ca. 453 Ma), slightly predating all known amalgamation timing derived independently from metamorphic and igneous dataset, because of the consequent lag time of the crustal response in the arc zone.

5.2.2. Subduction polarity of the NQO: south-dipping or north-dipping

Another tectonic controversy is whether the subduction polarity of the NQO was north- or south-dipping (Zuza et al., 2018). The northward subduction scenario would predict a south facing magmatic arc constructed north of the main suture within the SWNCB during the Cambrian-Ordovician. The Early Paleozoic magmatic plutons in the southern Alxa have been invoked as indicators for northward subduction polarity (Fu et al., 2020a). While in more views, this phase of plutonism is preferred to infer the southward subduction of the Paleo-Asian Ocean beneath the Alxa continental arc (Liu et al., 2016), raising an ambiguous debete. In the SWNCB, there is no sign of corresponding magmatism having been found. Furthermore, source interpretation shows that the CQT has obducted eastwards above the SWNCB. Otherwise, the southward thrusting of the SWNCB will require sources of the Lashizhong turbidites to contain a considerable amount of zircons from the uplifted SWNCB above a north-dipping suture zone and the foreland should be created in the CQT instead of the SWNCB.

Accordingly, our stratigraphic investigation approves for a southward subduction polarity for the NQO (Sobel & Arnaud, 1999; Gehrels et al., 2003a; Xiao et al., 2009; Dong et al., 2021). But, we do not mean to conclusively preclude the possibility of northward subduction of some oceans in the NQO as there may be multiple subduction systems between the SWNCB and the CQT.

5.2.3. Synchronous closure of the NQO at least in the east

The third tectonic uncertain can be addressed here is the process of the NQO closure. Almost all models on the NQO prefer a diachronous suturing mode (Xu et al., 2013a; Wu et al., 2016; Li et al., 2017; Zuza et al., 2018; Fu et al., 2021a). A sequence of basin-filling events triggered by the NQO closure occurred in the SWNCB, including forebulge flexural uplift (e.g., unconformity below the Kelimoli Formation), followed by rapid shallow shelf drowning to abyssal plain setting (e.g., the Kelimoli and

Wulalike formations), until the arrival and superimposition of turbidites from the west (e.g., the Lashizhong Formation). Evolution of these geologic activities of each stage was broadly synchronous over time in all sections (Figure 03), hinting at along-strike synchronicity of orogenic activities over a distance of ~800 km. Therefore, we here propose a strikingly distinct model that argues, at least in the east, the NQO was closed synchronously. Or, the closure of the NQO should be clockwise as its easternmost portion has an older closure age.

5.3. Ordovician tectono-sedimentary evolution of peripheral foreland in the SWNCB

The pre-Katian strata are characteristic of records of passive margin deposition, capped by a regionally traceable, nearly uninterrupted, carbonate shelf (Chen, 2011; Li et al. 2012; Wang et al., 2016b), which was fed by a small amount of quartzose influx from the craton interior to the northeast (Sun & Dong 2020a). The stable setting was punctuated by the initial CQT-NCB collision that spurred intense peripheral upwarp and basin reverse in the SWNCB, recorded by a stratigraphic break on top of the Zhuozishan Formation. This unconformity and correlative conformable contact separate passive margin sediments from overlying underfilled foreland fills with a distinctive type of megasequence formed in a more unstable tectonic setting (Figure 09d). The basin-filling process of peripheral foreland can be categorized into three distinct stages as expressed by three diverse lithological facies in ascending order.

Stage 1 (The Kelimoli Formation). Ongoing eastward outgrowth of CQT orogen wedge caused the SWNCB lithosphere to flex by depressing leading edge of the plate beneath it (Crampton & Allen, 1995) and created a zone of foredeep (e.g., the Qingliang Foredeep) in the study area triggered by flexural subsidence nearby. The tectonic load led to rapid drowning of the forebulge unconformity, recorded by basin deepening into a west-dipping carbonate slope at the distal foredeep (Figure 11). Given the flexural rigidity of the lithosphere, the eastern portion should have been uplifted as the forebulge where shallow carbonate platform sustained in the east (e.g., well Lucan 1; Figure 03).

Stage 2 (The Wulalke Formation). Forward passage of the flexural wave enhanced deepening of the distal foredeep and led to the cratonward migrating of carbonate slope-platform to the well Lucan 1 (Figure 03). The study area underwent a stage of starved sedimentation accompanied by fallout of volcanic ash cloud, with the abyssal accumulation of hemipelagic black shale that contains thin beds of laminated chert. Ongoing forebulge uplift finally led to large-scale erosion and destruction of the carbonate platform margin further to the east, as evidenced by the carbonate debrites. These carbonate breccias were resedimented

490 from underlying carbonate slope-platform sediments, and were transported downslope by gravitational
491 processes to deposition in the base-of-slope apron at the easternmost basin plain.
492 *Stage 3 (The Lashizhong Formation)*. The turbidites in the Xishan area are over 3000 meters thick,
493 reflecting the rather rapid topographic growth and erosion of the CQT, possibly due to intense crustal
494 thickening of the Qilian Orogen. Tectonic activities pushed terrigenous turdidity currents eastwards from
495 the high-elevation thrust wedge over the east-dipping slope until sitting depositionally on the abyssal plain.
496 Two respective detrital aprons from opposite landmasses comingled at abyssal depths on top of the abyssal
497 plain shales. It is interestingly to note that the Early Paleozoic zircons are infrequent in most of the
498 Lashizhong turbidites (besides the samples LSY and SGK03; Figure 09b), incompatible with the present
499 proportion of widely exposed Early Paleozoic plutons in the CQT. This inference hints at that much of
500 those intrusions have not been evlavetd to the surface to serve as sources during the initial collision. Yet, at
501 least in part, those rocks were rapidly uplifted to the crustal surface as local sources shedding sediments to
502 some drainage systems (e.g., SGK03 & LSY; Figure 09).
503 Collectively, during the very first suturing stage of the CQT-WNCB at ca. 453 Ma, an
504 eastward-expanding foredeep was constructed in the SWNCB when the orogenic wedge in the Qilian
505 Orogen expanded eastwards. Considerable subsidence was filled by the eastward progradation of westerly
506 turbiditic influxes superposing atop of the eastward-backsteeping carbonate platform-slope system (Figure
507 12).
508
509 **5.4. Implication for the early Paleozoic tectonic evolution of the ENQO**
510 The CQT along with other terranes that make up the present northern Tibet participated in the global
511 Rodinia assemblage, occupying a position at the northern Indo-Australian margin (Song et al., 2013; Fu et
512 al., 2019a) witnessed by the widespread ca. 950 Ma plutonism across the northern Tibet (Song et al., 2012;
513 Gehrels et al., 2003b; Wu et al., 2016, 2017b; Peng et al., 2019; Yu et al., 2021) and coeval deformation
514 (Zuza et al., 2018).
515 This spatial linkage probably sustained until the dispersal of the Rodinia at the late Neoproterozoic
516 (Song et al., 2010, 2013) before a sequence of break-up rifting events that ultimately isolated the northern
517 Tibetan terranes from the Indo-Australian margin at ca. 750 Ma. The rifting was recorded by ca. 830–600
518 Ma bimodal magmatism observed throughout the northern Tibet (Xu et al., 2015; Song et al., 2019b; Wu et
519 al., 2021a), leading to the opening of the Proto-Tethys Ocean that separated the Tarim, NCB, and northern

Tibetan terranes from the northern peripheral of the Gondwana (Huang et al., 2018; Zhao et al., 2018; Metcalfe, 2021).

In this period, these East Asian terranes, including the Tarim, NCB, as well as various micro-blocks that constitute the Central China Orogenic System, were located relatively adjacent to the Gondwana, and far away from the Siberia-Baltica-Laurasia landmass separated by the vast Paleo-Asian Ocean (Figure 13a; Xiao et al., 2003, 2015; Huang et al., 2018; Zhao et al., 2018). During the northward drift of these continental slivers, multiple Tethyan ocean basins formed, making the northern Proto-Tethys to be an archipelagic ocean (Figures 13a, b). Of these branches, the Shangdan-Kunlun Ocean is conventionally considered as the major branch separating the eastern Asian blocks from the Gondwana (Zhao et al., 2018; Dong et al., 2021). In the North Qilian Orogen, the oldest recognized Yushigou ophiolitic mélange yield high precise formation ages of ca.530–560 Ma (Qian *et al.*, 1998, 2001; Xia *et al.*, 2003; Smith & Yang, 2006; Xia & Song, 2010; Song *et al.*, 2013; Li *et al.*, 2017), and a west-dipping passive continental margin evolved in the SWNCB.

The proximity of the northern Tibetan terranes with the NCB is endorsed by comparisons of trilobite fossils (McKenzie et al., 2011; Myrow et al., 2015), litho-stratigraphy (Sun et al., 2014, 2019) and shelly faunas (Rong et al., 2003; Huang et al., 2018), making it more likely that the NQO was a relatively small ocean between the CQT and SWNCB as argued by Zuza et al. (2018). The shrinking of these oceans began at ca. 520 Ma, and the northern Tibetan terranes were bounded by a north-facing Qilian arc in the north and a south-facing Kunlun arc in the south, dispersed along the southern margin (present coordinate) of the NCB (Figures 12a&13c). Convergence between the CQT and the NCB was accomplished by a single south-dipping (present-day coordinate) convergent system (Sobel & Arnaud, 1999; Gehrels *et al.*, 2003a, 2003b; Xiao *et al.*, 2009; Wu *et al.*, 2016; Zuza *et al.*, 2018), as the SWNCB lacks plutonic rocks of this age with the formation of a passive continental margin that faced the NQO until Middle Ordovician (Sun & Dong, 2020a). Arc related plutonic rocks of ca.477–512 Ma (Wu *et al.*, 2004, 2006, 2010) and boninite massif of ca. 517 Ma imply that the southward subduction of the NQO should initiate at ca. 520 Ma (Song *et al.*, 2013; Fu et al., 2021a), leading to the conversion of an Atlantic-type passive margin into an Andean-type active margin in the CQT (Song et al., 2013).

Microslices in the northern Tibet were later accreted to and remained juxtaposed to a position at the southern flank of the NCB–Tarim (Yin & Harrison, 2000; Song et al., 2007, 2014, 2019a; Zhao et al., 2018; Yan et al., 2021; Fu et al., 2021a) by the closure of the NQO at ca. 453 Ma. The ribbon-like “Asiatic Hunic

550 superterrane" (Metcalfe, 2013, 2021; Stampfli et al., 2013) that comprises an assemblage of continental
551 blocks and intra-oceanic arcs including the NCB-Tarim and all terranes in the Central China Orogenic
552 System was amalgamated then (Figures 13d). The closure of these various branches of the Tethyan oceans,
553 including the Erlangping back-arc Ocean, N-Qilian Ocean, S-Qilian Ocean, N-Qaidam Ocean, and
554 Qimantage Ocean was nearly synchronous at ca. 450–445 Ma (Sun et al., 2021). This finding infers the
555 nearly coeval accretion of the North Qinling, CQT, Olongbuluke, Qaidam, and Central Kunlun at ca. 450–
556 445 Ma onto the NCB-Tarim, rather than sequential accretion from north to south, which would predict
557 progressively southward younging closure timing. The synchronous collision of the North Qinling and
558 CQT with the NCB is at odds with clockwise or counterclockwise rotation of the Qilian-Qaidam-Kunlun
559 terrane during the ocean closure, indicating presumably that the extent of these oceanic branches is
560 relatively narrow. Therefore, we favor a model that places the northern Tibetan terranes in the marginal sea
561 setting behind the Kunlun Arc.
562

563 ## 6. Conclusions

564 Our new data allow the following four major conclusions:
565 1) The Pre-Katian quartz arenite in the SWNCB were sourced from NCB basement to the east, and were
566 deposited in a passive margin setting in response to the spreading of the ENQO.
567 2) The Katian turbidites in both the SWNCB and the ENQAB have a common provenance from the CQT,
568 and show features of deposition in a collision-induced underfilled foreland basin.
569 3) The first arrival of the CQT-originated detritus above passive continental margin in the westernmost
570 NCB yields a solid constraint on the initial ENQO closure that the resulted the CQT-SWNCB collision
571 onset at ca. 453 Ma.
572 4) An eastward-expanding foredeep was constructed in the SWNCB during the eastward expansion of
573 the Qilian orogenic wedge. This foredeep was filled by the eastward progradation of turbiditic influxes
574 superposing on the eastward-backsteeping carbonate platform-slope.
575

576 ## Acknowledgement

The authors would like to acknowledge editors and referees for reviews and insightful comments that led to a better version of our work. The first author would like to express his appreciation to Prof. Yanlong Chen at Northwest University for kind suggestions on both field preparation and sedimentology. Financial support for this study was jointly given by the NSFC (Grants: 41930217, 42072260 and 41602109), Foundation of State Key Laboratory of Petroleum Resources and Prospecting, China University of Petroleum, Beijing (No. PRP/open-2007) and Natural Science Basic Research Program of Shaanxi (Program No. 2021JM-158).

Disclosure statement

No potential conflict of interest was reported by the authors.

Data Availability Statement

All data related to this manuscript, including sandstone modal composition, sampling location and detrital zircon U-Pb dating, have been fully submitted to and are available from the editorial board.

591 **References**

592 Aitchison, J. C., Badengzhu, A., Davis, M., Liu, J., Luo, H., Malpas, J. G., et al. (2000). Remnants of a
593 Cretaceous intra-oceanic subduction system within the Yarlung-Zangbo suture (southern Tibet). Earth
594 and Planetary Science Letters, 183(1–2), 231–244.
595 An, W., Hu, X., Garzanti, E., Wang, J. G., & Liu, Q. (2021). New precise dating of the India-Asia collision
596 in the Tibetan Himalaya at 61 Ma. Geophysical Research Letters, 48, e2020GL090641.
597 https://doi.org/10.1029/2020GL090641
598 Belousova, E., Griin, W., O'Reilly, S. Y., & Fisher, N. (2002). Igneous zircon: trace element composition as
599 an indicator of source rock type. Contributions to Mineralogy and Petrology, 143, 602–622.
600 https://doi.org/10.1007/s00410-002-0364-7
601 Bian, Q. T., Gao, S. L., Li, D. H., Ye, Z. R., Chang, C. F., & Luo, X. Q. (2001). A Study of the
602 Kunlun-Qilian-Qinling Suture System. Acta Geological Sinica-English Edition, 75, 364–374.
603 https://doi.org/10.1111/j.1755-6724.2001.tb00054.x
604 Black, L. P., Kamo, S. L., Allen, C. M., Aleinikof, J. N., Davis, D. W., Korsch, R. J., & Foudoulis, C.
605 (2003). TEMORA 1: a new zircon standard for phanerozoic U-Pb geochronology. Chemical Geology,
606 200, 155–170. https://doi.org/10.1016/S0009-2541(03)00165-7.
607 Cawood, P. A., Hawkesworth, C. J., & Dhuime, B. (2012). Detrital zircon record and tectonic setting.
608 Geology, 40(10), 875–878. https://doi.org/10.1130/G32945.1
609 Chang, C. F., Chen, N., Coward, M. P., Deng, W. M., Dewey, J. F., Gansser, A., Harris, B. W., Kidd, W. S.
610 F., Leeder, M. R., Li, H., Lin, J., Liu, C., Mei, H., Molnar, P., Pan, Y., Pearce, J. A., Shackleton, R. M.,
611 Smith, A. B., Sun, Y., Ward, M., Watts, D. R., Xu, J., Xu, R., Yin, J., & Zhang, Y. (1986). Preliminary
612 conclusions of the Royal Society and Academia Sinica 1985 geotraverse of Tibet. Nature, 323, 501–
613 507. https://doi.org/10.1038/323501a0
614 Charlotte, R., Benoit Petri, Jean-François, G., Gianreto, M., Federico, G., Garry, D. Karner, Patricio H.
615 Figueredo, Christopher, A. (2020). Johnson, Anne-Marie Karpoff. Tectono-sedimentary evolution of a
616 fossil ocean-continent transition: Tasna nappe, central Alps (SE Switzerland). Geological Society of
617 America Bulletin, 132 (7–8), 1427–1446. https://doi.org/10.1130/B35310.1
618 Chen, Q. (2011). Research on the lithofacies paleogeography of the Lower Paleozoic in the southwestern
619 margin of Ordos, (Doctoral dissertation). Northwest University (in Chinese with English abstract).
620 Chen, X., Bergström, S. M., Zhang, Y. D., & Wang, Z. H. (2013). A regional tectonic event of Katian (Late

621 Ordovician) age across three major blocks of China. Chinese Science Bulletin, 58, 4292–4299.
622 https://doi.org/10.1007/s11434-013-5990-0
623 Chen, Q., Li, W. H., Li. Z. C., Chen, G., Liu, X., & Li, M. (2020). Ordovician carbonate gravity deposition
624 in the southwestern margin of Ordos and its palaeogeographical significance. Journal of Northwest
625 University (Natural Science Edition), 50, 113–122 (in Chinese with English abstract).
626 Corfu, F., Hanchar, J. M., Hoskin, Paul W.O., Kinny, P. (2003). Atlas of Zircon Textures. Reviews in
627 Mineralogy and Geochemistry, 53 (1), 469–500. https://doi.org/10.2113/0530469
628 Crampton, S. L., & Allen, P. A. (1995). Recognition of forebulge unconformities associated with early stage
629 foreland basin development: Example from the North Alpine foreland basin. American Association of
630 Petroleum Geologists Bulletin, 79, 1495–1514.
631 https://doi.org/10.1306/7834DA1C-1721-11D7-8645000102C1865D
632 Cohen, K. M., Finney, S. C., Gibbard, P. L., & Fan, J. X. (2013). The ICS International Chronostratigraphic
633 Chart. Episodes, 36, 199–204. https://doi.org/10.18814/epiiugs/2013/v36i3/002
634 Darby, B. J., & Gehrels, G. (2006). Detrital zircon reference for the North China block. Journal of Asian
635 Earth Sciences, 26, 637–648. https://doi.org/10.1016/j.jseaes.2004.12.005
636 DeCelles, P. G., Kapp, P., Gehrels, G. E., & Ding, L. (2014). Paleocene-Eocene foreland basin evolution in
637 the Himalaya of southern Tibet and Nepal: Implications for the age of initial India-Asia collision.
638 Tectonics, 33, 824–849. https://doi.org/10.1002/2014TC003522
639 Dickinson, W. R. (1985). Interpreting provenance relations from detrital modes of sandstones. In: Zuffa GG
640 (Eds) Provenance of arenites (Vol. 148, pp. 333-361). Berlin, Springer Netherlands.
641 Dickinson, W. R., & Suczek, C. A. (1979). Plate tectonics and sandstone compositions. American
642 Association of Petroleum Geologists, 63, 2164–2182.
643 https://doi.org/10.1306/2F9188FB-16CE-11D7-8645000102C1865D
644 Domeier, M. (2018). Early Paleozoic tectonics of Asia: Towards a full-plate model. Geoscience Frontiers, 9,
645 789–862. https://doi.org/10.1016/j.gsf.2017.11.012
646 Dong, Y. P., & Santosh, M. (2016). Tectonic architecture and multiple orogeny of the Qinling Orogenic Belt,
647 Central China. Gondwana Research, 29, 1–40. https://doi.org/10.1016/j.gr.2015.06.009
648 Dong, Y. P., Zhang, G. W., Neubauer, F., Liu, X. M., Genser, J., & Hauzenberger, C. (2011). Tectonic
649 evolution of the Qinling orogen, China: review and synthesis. Journal of Asian Earth Sciences, 41,
650 213–237. https://doi.org/10.1016/j.jseaes.2011.03.002

651 Dong, C. Y., Wan, Y. S., Xu, Z. Y., Liu, D. Y., Yang, Z. S., Ma, M. Z., & Xie, W. Q. (2013). SHRIMP zircon
652 U-Pb dating of late Paleoproterozoic khondalites in the Daqing Mountain area on North China Craton.
653 Science China-Earth Sciences, 56, 115–125. https://doi.org/10.1007/s11430-012-4459-3
654 Dong, Y. P., Zhang, X. N., Liu, X. M., Li, W., Chen, Q., Zhang, G. W., Zhang, H. F., Yang, Z., Sun, S. S., &
655 Zhang, F. F. (2015). Propagation tectonics and multiple accretionary processes of the Qinling Orogen.
656 Journal of Asian Earth Sciences, 104, 84–98. https://doi.org/10.1016/j.jseaes.2014.10.007
657 Dong, Y. P., Neubauer, F., Genser, J., Sun, S. S., Yang, Z., Zhang, F. F., Cheng B., Liu, X. M., & Zhang, G.
658 W. (2018). Timing of Orogenic Exhumation Processes of the Qinling Orogen: Evidence From
659 $^{40}Ar/^{39}Ar$ Dating. Tectonics, 37, 4037–4046. https://doi.org/10.1029/2017TC004765
660 Dong, Y.P., He, D.F., Sun, S.S., Liu, X.M., Zhou, X.H., Zhang, F.F., Yang, Z., Cheng, B., Zhao, G.C., &
661 Li, J.H. (2018b). Subduction and accretionary tectonics of the East Kunlun orogen, western segment
662 of the Central China orogenic system. Earth-Science Reviews, 186, 231–261.
663 https://doi.org/10.1016/j.earscirev.2017.12.006
664 Dong, Y. P., Sun, S. S., Santosh, M., Zhao. J., Sun, J.P., He, D.F., Shi, X.H., Hui, B., Cheng, C., & Zhang,
665 G.W. (2021). Central China Orogenic Belt and amalgamation of East Asian continents. Gondwana
666 Research, 100, 131-194. https://doi.org/10.1016/j.gr.2021.03.006
667 Du, Y., Wang, J., Han, X., & Shi, G. R. (2003). From flysch to molasse-sedimentary and tectonic evolution
668 of late Caledonian-early Hercynian foreland basin in North Qilian Mountains. Journal of China
669 University of Geosciences, 14, 1–7 (in Chinese with English abstract).
670 Du, Y. S., Zhu, J., Xu, Y. J., Yang, J. H., & Huang, H. (2009). Research on the late Caledonian to early
671 Hercynian sedimentology of the North Qilian Orogen. China University of Geosciences Press, Wuhan
672 (in Chinese with English abstract).
673 Fan, R., Ma, X. Y., Lv, D., Lu, Y. Z., Zhang, X. L., Zhang, Y. D., Deng, S. W., Tan, C., Song, H. N., Zhang,
674 F. L., Li, X., Zhang, S. B., & Duan, W. Z. (2020). Upper Ordovician conodont and graptolite
675 biostratigraphy of Pingliang, Gansu Province, China. Acta Geological Sinica, 94, 3213–3227 (in
676 Chinese with English abstract).
677 Fei, A. W. (2001). Study of trace fossil assemblage and paleoenvironment of Middle Ordovician
678 Lashizhong Formation, Ordos Basin. Geological Journal of China Universities, 7(3), 278–287 (in
679 Chinese with English abstract).
680 Fei, A. W., Liu, C. L., Gan, J., Zhang, Z. T. (2004). Bioturbation structures and paleogeography of mixed

681 deposits of the Lower Ordovician Sandaokan Formation, Ordos basin. Geology in China, 31(4), 347–
682 355 (in Chinese with English abstract).
683 Feng, Z. Z., Zhang, Y. S., Jin, Z. K. (1998). Type, origin, and reservoir characteristics of dolostones of the
684 Ordovician Majiagou Group, Ordos, North China Platform. Sedimentary Geology, 118 (1–4), 127–140.
685 https://doi.org/10.1016/S0037-0738(98)00009-8
686 Varejão, F.G., Warren, L.V., Simões, M.G., Buatois, L.A., Mángano, M.G., Bahniuk Rumbelsperger, A.
687 M., & Assine, M. L. (2021). Mixed siliciclastic–carbonate sedimentation in an evolving epicontinental
688 sea: Aptian record of marginal marine settings in the interior basins of north-eastern Brazil.
689 Sedimentology, 68, 2125–2164. https://doi.org/10.1111/sed.12846
690 Fu, L. P., Hu, Y. X., Zhang, Z. F., & Wang, S. X. (1993). The mark on the ecology of sedimentarial
691 environment in middle and upper Ordovician at Ordos Basin. Northwest Geoscience, 2, 1–88 (in
692 Chinese with English abstract).
693 Fu, C. L., Yan, Z.,Wang, Z. Q., Buckman, S., Aitchison, J. C., Niu, M. L., Cao, B., Guo, X. Q., Li, X. C.,
694 Li, Y. S., Li, J. L. (2018). Lajishankou Ophiolite Complex: implications for Paleozoic multiple
695 accretionary and collisional events in the South Qilian Belt. Tectonics, 37, 1321–1346.
696 https://doi.org/10.1029/2017TC004740
697 Fu, D., Kusky, T., Wilde, S. A., Polat, A., Huang, B., & Zhou, Z. P. (2019a). Early Paleozoic
698 collision-related magmatism in the eastern North Qilian orogen, northern Tibet: A linkage between
699 accretionary and collisional orogenesis. Geological Society of America Bulletin, 131(5–6), 1031–1056.
700 https://doi.org/10.1130/B35009.1
701 Fu, C. L., Yan, Z., Guo, X. Q., Niu, M. L., Cao, B., Wu, Q., Li, X. C., Wang, Z. Q. (2019b). Assembly and
702 dispersal history of continental blocks within the Altun-Qilian-North Qaidam mountain belt, NW
703 China. International Geology Review, 61, 424–447. https://doi.org/10.1080/00206814.2018.1428831
704 Fu, C. L., Yan, Z., Aitchison, J. C., Guo, X. Q., Xia, W. J. (2019c). Abyssal and suprasubduction
705 peridotites in the Lajishan Ophiolite Belt: implication for initial Subduction of the Proto-Tethyan
706 Ocean. The Journal of Geology, 127, 393–410. https://doi.org/10.1086/703488
707 Fu, D., Kusky, T. M., Wilde, S. A., Windley, B. F., Polat, A., Huang, B., & Zhou, Z. (2020a). Structural
708 anatomy of the early Paleozoic Laohushan ophiolite and subduction complex: Implications for
709 accretionary tectonics of the Proto-Tethyan North Qilian orogenic belt, northeastern Tibet. Geological
710 Society of America Bulletin, 132, 2175–2201. https://doi.org/10.1130/B35442.1

711 Fu, C. L., Yan, Z., Aitchison, J. C., et al. (2020b). Multiple subduction processes of the Proto-Tethyan
712 Ocean: Implication from Cambrian intrusions along the North Qilian suture zone. Gondwana Research,
713 87 (2020), 207–223. https://doi.org/10.1016/j.gr.2020.06.007
714 Fu, D., Huang, B., Johnson, T. E., Wilde, S. M., Jourdan, F., Polat, A., Windley, B., Hu, Z. C., Kusky, T.
715 (2021a). Boninitic blueschists record subduction initiation and subsequent accretion of an arc-forearc
716 in the northeast Proto-Tethys Ocean. Geology. https://doi.org/10.1130/G49457.1
717 Fu, C. L., Yan, Z., Aitchison, J. C., Xiao, W. J., Buckman, S., Wang, B. Z., Zhai, Q. G., Cao, B. (2021b).
718 Short-lived intra-oceanic arc-trench system in the North Qaidam belt (NW China) reveals complex
719 evolution of the Proto-Tethyan Ocean. Geological Society of America Bulletin.
720 https://doi.org/10.1130/B36127.1
721 Gao, Z. Z., Luo, S. S., He, Y. B., Zhang, J. S., & Tang, Z. J. (1995). The middle Ordovician contourite on
722 the west margin of Ordos. Acta Sedimentologica Sinica, 13, 16–26 (in Chinese with English abstract).
723 Garzanti, E., Baud, A., & Mascle, G. (1987). Sedimentary record of the Northward flight of India and its
724 collision with Eurasia (Ladakh Himalaya, India). Geodinamica Acta, 1(4–5), 297–312.
725 https://doi.org/10.1080/09853111.1987.11105147
726 Gehrels, G. E., Yin, A., & Wang, X. F. (2003a). Detrital-zircon geochronology of the northeastern Tibetan
727 plateau. Geological Society of America Bulletin, 115(7), 881–896.
728 https://doi.org/10.1130/0016-7606(2003)115<0881:dgotnt>2.0.co;2
729 Gehrels, G. E., Yin, A., & Wang, X. F. (2003b). Magmatic history of the northeastern Tibetan Plateau.
730 Journal of Geophysical Research, 108(B9). https://doi.org/10.1029/2002jb001876
731 Gehrels, G., Kapp, P., DeCelles, P., Pullen, A., Blakey, R., Weislogel, A., et al. (2011). Detrital zircon
732 geochronology of pre-Tertiary strata in the Tibetan-Himalayan orogen. Tectonics, 30(5), TC5016.
733 https://doi.org/10.1029/2011tc002868
734 Guo, J. J., Zhao, F. Q., & Li, H. K. (1999). Jinningian collisional granite belt in the eastern sector of the
735 central Qilian massif and its implication. Acta Geological Sinica, 10, 10–15 (in Chinese with English
736 abstract).
737 Guo, Y. R., Zhao, Z. Y., Fu, J. H., Xu, W. L., Shi, X. Y., Sun, L. Y., Liu, H. (2012). Sequence lithofacies
738 paleogeography of the Ordovician in Ordos Basin, China. Acta Petrologica Sinica, 33, 95–109 (in
739 Chinese with English abstract).
740 Hu, X. M., Sinclair, H. D., Wang, J. G., Jiang, H. H., & Wu, F. Y. (2012). Late Cretaceous-Palaeogene

741 stratigraphic and basin evolution in the Zhepure Mountain of southern Tibet: implications for the
742 timing of India-Asia initial collision. Basin Research, 24, 520–543.
743 https://doi.org/10.1111/j.1365-2117.2012.00543.x
744 Hu, X., Garzanti, E., Moore, T., & Raffi, I. (2015). Direct stratigraphic dating of India-Asia collision onset
745 at the Selandian (middle Paleocene, 59 ± 1 Ma). Geology, 43(10), 859–862.
746 https://doi.org/10.1130/G36872.1
747 Hu, X. M., Garzanti, E., Wang, J. G., Huang, W. T., An, W., & Webb, A. (2016). The timing of India-Asia
748 collision onset-Facts, theories, controversies. Earth-Science Reviews, 160, 264–299.
749 https://doi.org/10.1016/j.earscirev.2016.07.014
750 Huang, B. C., Yan, Y. G., Piper, J. D. A., Zhang, D. H., Yi, Z. Y., Yu, S., & Zhou, T. H. (2018).
751 Paleomagnetic constraints on the paleogeography of the East Asian blocks during Late Paleozoic and
752 Early Mesozoic times. Earth-Science Review, 186, 8–36.
753 https://doi.org/10.1016/j.earscirev.2018.02.004
754 Ingersoll, R. V., Fullard, T. F., Ford, R. L., Grimm, J. P., Pickle, J. D., & Sares, S. W. (1984). The effect of
755 grain size on detrital modes: A test of the Gazzi-Dickinson point-counting method. Journal of
756 Sedimentary Research, 54(1), 103–116.
757 https://doi.org/10.1306/212F83B9-2B24-11D7-8648000102C1865D
758 Jian, P., Kröner, A., Windley, B. F., Zhang, Q., Zhang, W., & Zhang, L. Q. (2012). Episodic mantle
759 melting-crustal reworking in the late Neoarchean of the northwestern North China Craton: Zircon ages
760 of magmatic and metamorphic rocks from the Yinshan Block. Precambrian Research, 222–223, 230–
761 254. https://doi.org/10.1016/j.precamres.2012.03.002
762 Jing, X. C., Zhou, H. R., & Wang, X. L. (2015). Ordovician (middle Darriwilian-earliest Sandbian)
763 conodonts from the Wuhai area of Inner Mongolia, North China. Journal of Paleontology, 89, 768–790.
764 https://doi.org/10.1017/jpa.2015.54
765 Jing, X. C., Zhou, H. R., Wang, X. L., Yang, Z. H., Fang, Q., Wang, Z. T., & Fan, J. (2020). A review on
766 Ordovician conodont biostratigraphy in North China Plate and new advances in its northwestern
767 margin. Earth Science Frontiers, 27, 199–212 (in Chinese with English abstract).
768 Kang, Y. (2021). Tectonic paleogeography of Early Paleozoic and its significances for petroleum
769 exploration in the west and south of Ordos block. Doctoral dissertation, Northwest University, 1–156
770 (in Chinese with English abstract).

771 Li, Z. H. (2018). Paleozoic tectonic evolution in the Helanshan Tectonic Belt: Constraints from U-Pb
772 geochronology of detrital zircon. Doctoral dissertation, Northwest University, 1–97 (in Chinese with
773 English abstract).
774 Li, X. P., Yang, Z. Y., Zhao, G. C., Grapes, R., & Guo, J. H. (2011). Geochronology of khondalite-series
775 rocks of the Jining Complex: confirmation of depositional age and tectonometamorphic evolution of
776 the North China Craton. International Geology Review, 53, 1194–1211.
777 https://doi.org/10.1080/00206810903548984
778 Li, W. H., Chen, Q., Li, Z. Y., Wang, R. G., Wang, Y., & Ma, Y. (2012). Lithofacies palaeogeography of the
779 Early Paleozoic in Ordos area. Journal of Palaeogeography, 14, 85–90 (in Chinese with English
780 abstract).
781 Li, Z. H., Xu, L. M., Liu, X. S., Yuan, X. Q., & Hu, J. M. (2015). Critical timing of sedimentary filling
782 records o Ordovician and its tectonic significance on the southern Ordos Basin. Chinese Journal of
783 Geology, 50, 428–445 (in Chinese with English abstract).
784 https://doi.org/10.3969/j.issn.0563-5020.2015.006
785 Li, S. Z., Li, T., Zhao, S. T., Li, X. Y., Liu, X., Guo, L. L., Yu, S. Y., & Li, S. J. (2017). Proto Tethys Ocean
786 in East Asia (V): Attribute of continental margin and microcontinental assembly in the west segment
787 of the northern Proto Tethys Tectonic Domain. Acta Petrologica Sinica, 33, 1633–1652 (in Chinese
788 with English abstract).
789 Li, S. Z., Zhao, S. J., Liu, X., Cao, H. H., Yu, S., Li, X. Y., Somerville, I., Yu, S. Y., & Suo, Y. H. (2018a).
790 Closure of the Proto-Tethys Ocean and Early Paleozoic amalgamation of microcontinental blocks in
791 East Asia. Earth-Science Reviews, 186, 37–75. https://doi.org/10.1016/j.earscirev.2017.01.011
792 Li, Y. L., Tong, X., Zhu, Y. H., Lin, J. W., Zheng, J. P., Brouwer, F. M. (2018b).Tectonic affinity and
793 evolution of the Precambrian Qilian block: Insights from petrology, geochemistry and geochronology
794 of the Hualong Group in the Qilian Orogen, NW China. Precambrian Research, 315, 179–200.
795 https://doi.org/10.1016/j.precamres.2018.07.025
796 Li, W. H., Zhang, Q., Chen, Q., Li, K. Y, Guo, Y. Q., Yuan, Z., Ma, Y., Li, Z. Y., Bai, J. L., & Yang, B.
797 (2020). Sedimentary evolution of Early Paleozoic in Ordos Basin and its adjacent Areas. Journal of
798 Northwest University (Natural Science Edition), 50, 456–479 (in Chinese with English abstract).
799 Li, W. J., Chen, J. T., Hakim, A. J., Myrow, P. M. (2021). Middle Ordovician mass-transport deposits from
800 western Inner Mongolia, China: Mechanisms and implications for basin evolution. Sedimentology

https://doi.org/ 10.1111/sed.12949.

Liou, J. G., Wang, X., & Coleman, R. G., Zhang, Z. M., & Maruyama, S. (1989). Blueschists in major suture zones of China. Tectonics, 8, 609–619. https://doi.org/10.1029/TC008i003p00609

Liu, S. F., Steel, R., & Zhang, G. W. (2005). Mesozoic sedimentary basin development and tectonic implication, northern Yangtze Block, eastern China: Record of continent-continent collision. Journal of Asian Earth Sciences, 25, 9–27. https://doi.org/10.1016/j.jseaes.2004.01.010

Liu, Y. J., Neubauer, F., Genser, J., Takasu, A., Ge, X. H., & Handler, R. (2006). $^{40}Ar/^{39}Ar$ ages of blueschist facies pelitic schists from Qingshuigou in the Northern Qilian Mountains, western China. Island Arc, 15, 187–198. https://doi.org/10.1111/j.1440-1738.2006.00508.x

Liu, X. M., Gao, S., Diwu, C. R., Yuan, H. L., & Hu, Z. C. (2007). Simultaneous in-situ, determination of U-Pb age and trace elements in zircon by LA-ICP-MS in 20 μm spot size. Chinese Science Bulletin, 52(9), 1257–1264. http://dx.doi.org/10.1007/s11434-007-0160-x

Liu, S. F., Qian, T., Li, W. P., Dou, G. X., & Wu, P. (2015). Oblique closure of the northeastern Paleo-Tethys in central China. Tectonics, 34, 413–434. https://doi.org/10.1002/2014TC003784

Liu, Q., Zhao, G., Sun, M., Han, Y., Eizenhofer, P. R., Hou, Zhang, X. R., Zhu, Y. L., Wang, B., Liu, D, X., Xu, B. (2016). Early Paleozoic subduction processes of the Paleo-Asian Ocean: Insights from geochronology and geochemistry of Paleozoic plutons in the Alxa Terrane. Lithos, 262, 546–560. https://doi.org/10.1016/j.lithos.2016.07.041

Liu, X. G., Li, S. Z., Li, X. Y., Zhao, S. J., Wang, T. S., Yu, S. Y., Dai, L. M., Zhou, Z. Z., & Guo, R. H. (2018a). Detrital zircon U-Pb geochronology and provenance of the Sanxiatian Formation, Huade Group, in North China Craton: Implications for the breakup of the Columbia Supercontinent. Precambrian Research, 310, 305-319. https://doi.org/10.1016/j.precamres.2018.02.006

Liu, C. F., Wu, C., Zhou, Z. G., Yan, Z., Jiang, T., Song, Z. J., Liu, W. C., Yang, X., & Zhang, H. Y. (2018b). U-Pb detrital zircon geochronology from the basement of the Central Qilian Terrane: implications for tectonic evolution of northeastern Tibetan Plateau. International Journal of Earth Sciences, 107, 673–686. https://doi.org/10.1007/s00531-017-1522-5

Liu, X. G., Zhang, J., Li, S. Z., Li, X. Y., & Yin, C. Q. (2020). Tectono-sedimentary evolution of the Mesoproterozoic basins in the southern Yan-Liao and Mianchi-Queshan areas: insights from stratigraphic pattern and detrital zircon geochronology. International Journal of Earth Sciences, 109, 43–62. https://doi.org/10.1007/s00531-019-01784-w

Liu, X. G., Zhang, J., Yin, C. Q., Li, S. Z., Liu, J., Qian, J. H., & Zhao, C. (2021). A synthetic geochemical and geochronological dataset of the Mesoproterozoic sediments along the southern margin of North China Craton: Unraveling a prolonged peripheral subduction involved in breakup of Supercontinent Columbia. Precambrian Research, 357, 106154. https://doi.org/10.1016/j.precamres.2021.106154.

Mount, J. F. (1984). Mixing of siliciclastic and carbonate sediments in shallow shelf environments. Geology, 12 (7), 432–435. https://doi.org/10.1130/0091-7613(1984)12%3C432:MOSACS%3E2.0.CO;2

Ma, Z. R., Bai, H. F., Liu, B. X., Wang, H. W., & Chen, D. S. (2013). Lithofacies palaeogeography of the Middle-Late Ordovician Kelimoli and Wulalike ages in western Ordos area. Journal of Palaeogeography, 15, 751–764 (in Chinese with English abstract).

McKenzie, N. R., Hughes, N. C., Myrow, P. M., Choi, D. K., Park, T. Y. (2011). Trilobites and zircons link north China with the eastern Himalaya during the Cambrian. Geology, 39(6), 591–594. https://doi.org/10.1130/G31838.1

Metcalfe, I. (2013). Gondwana dispersion and Asian accretion: Tectonic and palaeogeographic evolution of eastern Tethys. Journal of Asian Earth Sciences, 66(8), 1–33. https://doi.org/10.1016/j.jseaes.2012.12.020

Metcalfe, I. (2021). Multiple Tethyan ocean basins and orogenic belts in Asia. Gondwana Research, 100, 87–130. https://doi.org/10.1016/j.gr.2021.01.012

Myrow, P. M., Chen, J., Snyder, Z., Leslie, S., Fike, D. A., Fanning, C. M., et al. (2015). Depositional history, tectonics, and provenance of the Cambrian-Ordovician boundary interval in the western margin of the North China block. Geological Society of America Bulletin, 127(9-10), 1174–1193. https://doi.org/10.1130/b31228.1

Pan, G. T., Ding, J., Yao, D., & Wang, L. Q. (2004). Geological Map of Qinghai-Xizang, Tibet, Plateau and Adjacent Areas, scale 1:1,500,000, Chengdu Cartographic Publishing House, 1–101 Chengdu, (In Chinese).

Pan, G. T., Wang, L. Q., Li, R. S., Yuan, S. H., Ji, W. H., Yin, F. G., Zhang, W. P., & Wang., B. D. (2012). Tectonic evolution of the Qinghai-Tibet Plateau. Journal of Asian Earth Sciences, 53, 3–14. https://doi.org/10.1016/j.jseaes.2011.12.018

Peng P. (2015). Late Paleoproterozoic-Neoproterozoic (1800–541 Ma) mafic dyke swarms and rifts in North China. In Zhai, M.G., (Eds.), Precambrian Geology of China (pp. 174–201). Berlin Heidelberg:

Springer.

Peng, P., Bleeker, W., Ernst, R. E., Soderlund, U., & McNicoll, V. (2011). U-Pb baddeleyite ages, distribution and geochemistry of 925 Ma mafic dykes and 900 Ma sills in the North China Craton: Evidence for a Neoproterozoic mantle plume. Lithos, 127, 210–221. https://doi.org/10.1016/j.lithos.2011.08.018

Peng, Y. B., Yu, S. Y., Li, S. Z., Zhang, J. X., Liu, Y. J., Li, Y. S., & Santosh, M. (2019). Early Neoproterozoic magmatic imprints in the Altun-Qilian-Kunlun region of the Qinghai-Tibet plateau: Response to the assembly and breakup of Rodinia supercontinent. Earth-Science Reviews, 199, 102954. https://doi.org/10.1016/j.earscirev.2019.102954

Perera, S., & Aitchison, J. C. (2021). Late Sandbian (Sa2) radiolarians of the Pingliang Formation from the Guanzhuang section, Gansu Province, China. Journal of Paleontology DOI: 10.1017/jpa.2021.86

Pettijohn, F.J. (1975). Sedimentary Rocks, Third edn. Harper and Row, New York.

Qian, Q., Wang, Y. M., Li, H. M., Jia, X. Q., Han, S., & Zhang, Q. (1998). Geochemical characteristics and genesis of diorites from Laohushan. Gansu Province. Acta Petrologica Sinica, 14, 520–528 (in Chinese with English abstract).

Qian, Q., Zhang, Q., & Sun, X. M. (2001). Tectonic setting and mantle source characteristics of Jiugequan basalts., North Qilian: constraints from trace elements and Nd-isotopes. Acta Petrologica Sinica, 17, 385–394 (in Chinese with English abstract).

Qian, T., Wang, Z. X., Wang, Y., Liu, S. F., Gao, W. L., & Li, W. P. (2021). Jurassic evolution of the Qaidam Basin in western China: Constrained by stratigraphic succession, detrital zircon U-Pb geochronology and Hf isotope analysis. Geological Society of America Bulletin, 133(11–12), 2291–2318. https://doi.org/10.1130/B35757.1

Sinclair, H. D. (1997). Tectonostratigraphic model for underfilled peripheral foreland basins: An Alpine perspective. GSA Bulletin, 109, 324–346. https://doi.org/10.1130/0016-7606(1997)109<0324:TMFUPF>2.3.CO;2

Smith, A. D., & Yang, H. Y. (2006). The neodymium isotopic and geochemical composition of serpentinites from ophiolitic assemblages in the Qilian fold belt, northwest China. Journal of Asian Earth Sciences, 28, 119–132. https://doi.org/10.1016/j.jseaes.2005.09.013

Sobel, E. R., & Arnaud, N. (1999). A possible middle Paleozoic suture in the Altyn Tagh, NW China. Tectonics, 18(1), 64–74. https://doi.org/10.1029/1998tc900023

Song, S. G. (1997). Tectonic evolution of subductive complex belts in the North Qilian Mountains. Advances in Earth Science, 12, 351–365 (in Chinese with English abstract).

Song, S. G., Zhang, L. F., Niu, Y. L., Su, L., Song, B., & Liu, D. Y. (2006). Evolution from oceanic subduction to continental collision: a case study of the Northern Tibetan Plateau inferred from geochemical and geochronological data. Journal of Petrology, 47, 435–455. https://doi.org/10.1093/petrology/egi080

Song, S. G., Zhang, L. F., Niu, Y. L., Wei, C. J., Liou, J. G., & Shu, G. M. (2007). Eclogite and carpholite-bearing meta-pelite in the North Qilian suture zone, NW China: implications for Paleozoic cold oceanic subduction and water transport into mantle. Journal of Metamorphic Geology, 25, 547–563.

Song, S. G., Su, L., Li, X. H., Zhang, G. B., Niu, Y. L., & Zhang, L. F. (2010). Tracing the 850-Ma continental flood basalts from a piece of subducted continental crust in the North Qaidam UHPM belt, NW China. Precambrian Research, 183, 805–816. https://doi.org/10.1016/j.penerecamres.2010.09.008

Song, S. G., Su, L., Li, X. H., Niu, Y. L., & Zhang, L. F. (2012). Grenville-age orogenisis in the Qaidam-Qilian block: The link between South China and Tarim. Precambrian Research, 220, 9–22. https://doi.org/10.1016/j.precamres.2012.07.007.

Song, S. G., Niu, Y. L., Su, L., & Xia, X. H. (2013). Tectonics of the North Qilian orogen, NW China. Gondwana Research, 23, 1378–1401. https://doi.org/10.1016/j.gr.2012.02.004

Song, S. G., Niu, Y. L., Su, L., Zhang, C., & Zhang, L. (2014). Continental orogenesis from ocean subduction, continent collision /subduction, to orogen collapse, and orogen recycling: The example of the North Qaidam UHPM belt, NW China. Earth-Science Reviews, 129, 59–84. https://doi.org/10.1016/j.earscirev.2013.11.010.

Song, S. G., Yang, L. M., Zhang, Y. Q., Niu, Y. L., Wang, C., Su, L., & Gao, Y. L. (2017). Qi-Qin accretionary belt in Central China Orogen: Accretion by trench jam of oceanic plateau and formation of intra oceanic arc in the Early Paleozoic Qin-Qi-Kun Ocean. Science Bulletin, 62, 1035–1038 (in Chinese with English abstract).

Song, S. G., Wu, Z. Z., Yang, L. M., Su, L., Xia, X. H., Wang, C., Dong, J. L., Zhou, C. A., & Bi, H. Z. (2019a). Ophiolite belts and evolution of the Proto-Tethys Ocean in the Qilian Orogen. Acta Petrologica Sinica, 35, 2948–2970. (in Chinese with English abstract).

Song, S. G., Niu, Y. L., Zhang, G. B., & Zhang, L. F. (2019b). Two epochs of eclogite metamorphism link

'cold' oceanic subduction and 'hot' continental subduction, the North Qaidam UHP belt, NW China. in Zhang, L.F., Zhang, Z., Schertl, H.P., & Wei, C.J. (Eds.), HP-UHP Metamorphism and Tectonic Evolution of Orogenic Belts (Vol. 474, pp. 275–289). Geological Society, London, Special Publication 474. https://doi.org/10.1144/SP474.2

Stampfli, G. M., Hochard, C., Vérard, C.,Wilhem, C., von Raumer, J. (2013). The formation of Pangea. Tectonophysics, 593, 1–19. https://doi.org/10.1016/j.tecto.2013.02.037

Sun, J. P., & Dong, Y. P. (2019a). Middle-Late Triassic sedimentation in the Helanshan Tectonic Belt: constrain on the tectono-sedimentary evolution of the Ordos Basin, North China. Geoscience Frontiers, 10, 213–227. https://doi.org/10.1016/j.gsf.2018.05.017

Sun, J. P., & Dong, Y. P. (2019b). Triassic tectonic interactions between the Alxa Massif and Ordos Basin: evidence from integrated provenance analyses on sandstones, North China. Journal of Asian Earth Sciences, 169, 162–181. https://doi.org/10.1016/j.jseaes.2018.08.002

Sun, J. P., & Dong, Y. P. (2019c). Cambrian tectonic evolution of the northwestern Ordos Terrane, North China: constraints of stratigraphy, sedimentology and zircon U-Pb geochronology. International Journal of Earth Sciences, 108, 569–586. https://doi.org/10.1007/s00531-018-1669-8

Sun, J. P., & Dong, Y. P. (2020a). Ordovician tectonic shift in the western North China Craton constrained by stratigraphic and geochronological analyses. Basin Research, 32, 1413–1440. https://doi.org/10.1111/bre.12435

Sun, J. P., & Dong, Y. P. (2020b). Stratigraphy and geochronology of Permo-Carboniferous strata in the Western North China Craton: Insights into the tectonic evolution of the southern Paleo-Asian Ocean. Gondwana Research, 88, 1–219. https://doi.org/10.1016/j.gr.2020.08.005

Sun, J. P., Dong, Y. P., Ma, L. C., Peng, Y., Chen, S. Y., Du, J. J., & Jiang, W. (2019). Late Paleoproterozoic tectonic evolution of the Olongbuluke Terrane, northern Qaidam, China: Constraints from stratigraphy and detrital zircon geochronology. Precambrian Research, 331, 105349. https://doi.org/10.1016/j.precamres.2019.105349

Sun, J. P., Dong, Y. P., Jiang, W., Ma, L. C., Chen, S. Y., Du, J. J., & Peng, Y. (2020). Reconstructing the Olongbuluke Terrane (northern Tibet) in the end-Neoproterozoic to Ordovician Indian margin of Gondwana. Precambrian Research, 348, 105865. https://doi.org/10.1016/j.precamres.2020.105865

Sun, J. P., Dong, Y. P., Ma, L. C., Chen, S. Y., Jiang, W. (2021). Devonian to Triassic tectonic evolution and basin transition in the East Kunlun−Qaidam area, northern Tibetan Plateau: Constraints from

951 stratigraphy and detrital zircon U−Pb geochronology. Geological Society of America Bulletin.
952 https://doi.org/10.1130/B36147.1
953 Tseng, C. Y., Yang, H. Y., Wan, Y., Liu, D., Wen, D. J., Lin, T. C., & Tung, K. A. (2006). Finding of
954 Neoproterozoic (775 Ma) magmatism recorded in metamorphic complexes from the North Qilian
955 orogen: evidence from SHRIMP zircon U-Pb dating. Chinese Science Bulletin, 51, 963–970 (in
956 Chinese with English abstract).
957 Tseng, C. Y., Yang, H. J., Yang, H. Y., Liu, D. Y., Wu, C. L., Cheng, C. K., Chen, C. H., & Ker, C. M.
958 (2009). Continuity of the North Qilian and North Qinling orogenic belts, Central Orogenic System of
959 China: evidence from newly discovered Paleozoic adakitic rocks. Gondwana Research, 16, 285–293.
960 https://doi.org/10.1016/j.gr.2009.04.003
961 Tung, K. A., Yang, H. J., Yang, H. Y., Liu, D. Y., Zhang, J. X., Wan, Y. S., & Tseng, C. Y. (2007a). SHRIMP
962 U-Pb geochronology of the zircons from the Precambrian basement of the Qilian Block and its
963 geological significances. Chinese Science Bulletin, 52, 2687–2701 (in Chinese with English abstract).
964 Tung, K. A., Yang, H. Y., & Liu, D. Y. (2007b). SHRIMP U-Pb geochronology of detrital zircons from the
965 Longshoushan Group and its tectonic significance. Chinese Science Bulletin, 52, 1414–1425 (in
966 Chinese with English abstract).
967 Tung, K. A., Yang, H. Y., Liu, D. Y., Zhang, J. X., Yang, H. J., Shau, Y. H., & Tseng, C. Y. (2013). The
968 Neoproterozoic granitoids from the Qilian Block, NW China: evidence for a link between the Qilian
969 and South China Cratons. Precambrian Research, 235, 163–189.
970 Tung, K. A., Yang, H. Y., Yang, H. J., Smith, A., Liu, D. Y., Zhang, J. X., Wu, C. L., Shau, Y. H., Wen, D. J.,
971 & Tseng, C. Y. (2016). Magma sources and petrogenesis of the early-middle Paleozoic backarc
972 granitoids from the central part of the Qilian block, NW China. Gondwana Research, 38, 197–219.
973 https://doi.org/10.1016/j.gr.2015.11.012
974 Wan, Y., Xie, H., Yang, H., Wang, Z., Liu, D., Kröner, A., Wilde, S. A., Geng, Y., Sun, L., Ma, M., Liu, S.,
975 Dong, C., & Du, L. (2013). Is the Ordos block Archean or Paleoproterozoic in age? Implications for
976 the Precambrian evolution of the North China Craton. American Journal of Science, 313(7), 683–711.
977 https://doi.org/10.2475/07.2013.03
978 Wang, Y. S., & Chen, J. N. (1987). Metamorphic zones and metamorphism in Qinghai Province and its
979 adjacent areas. Geological Publishing House, Beijing (in Chinese with English abstract).
980 Wang, Z. H., Bergström, S. M., Zhen, Y. Y., Chen, X., & Zhang, Y. D. (2013). On the integration of

Ordovician conodont and graptolite biostratigraphy: New examples from Gansu and Inner Mongolia in China. Alcheringa, 37, 510–528. https://doi.org/10.1080/03115518.2013.805491

Wang, Z. T., Zhou, H. R., Wang, X. L., Jing, X. C., & Zhang, Y. S. (2015). Volcanic event records at the southwestern Ordos Basin: The message from geochemical and zircon U-Pb geochronology of K-bentonites from Pingliang Formation, Shananxi and Gansu region. Acta Petrologica Sinica, 31, 2633–2654 (in Chinese with English abstract).

Wang, Z. H., Zhen, Y. Y., Zhang, Y. D., & Wu, R. C. (2016a). Review of the Ordovician conodont biostratigraphy in the different facies of North China. Journal of Stratigraphy, 40, 1–16 (in Chinese with English abstract).

Wang, Z. T., Zhou, H. R., Wang, X. L., Zheng, M. P., Santosh, M., & Jing, X. C. (2016b). Detrital zircon fingerprints link western North China Craton with east Gondwana during Ordovician. Gondwana Research, 40, 58–76. https://doi.org/10.1016/j.gr.2016.08.007

Wang, Z., Fan, R. Y., Zong, R. W., Gong, Y. M. (2021a). Middle Ordovician bottom current deposits in the western margin of the North China craton: Evidence from sedimentary and magnetic fabrics. Sedimentology https://doi.org/10.1111/sed.12957

Wu, C. L., Yang, J. S., Yang, H. Y., Wooden, J., Shi, R. D., Chen, S. Y., & Zheng, Q. G. (2004). Dating of two types of granite from North Qilian, China. Acta Petrologica Sinica, 20, 425–432 (in Chinese with English abstract).

Wu, C. L., Yao, S., Zeng, L., Yang, J., Wooden, J., Chen, S., & Mazadab, F. (2006). Double subduction of the early Paleozoic North Qilian oceanic plate: Evidence from granites in the central segment of North Qilian, NW China. Geology in China, 33, 1197–1208 (in Chinese with English abstract).

Wu, C. L., Xu, X. Y., Gao, Q. M., Li, X. M., Lei, M., Gao, Y. H., Frost, B. R., & Wooden, J. (2010). Early Palaeozoic granitoid magmatism and tectonic evolution in North Qilian, NW China. Acta Petrologica Sinica, 26, 1027–1044 (in Chinese with English abstract).

Wu, C., Yin, A., Zuza, A. V., Zhang, J., Liu, W., & Ding, L. (2016). Pre-Cenozoic geologic history of the central and northern Tibetan Plateau and the role of Wilson cycles in constructing the Tethyan orogenic system. Lithosphere, 8(3), 254–292. https://doi.org/10.1130/l494.1

Wu, S. J., Zhang, Y. S., Xing, E. Y. (2017a). Zircon U-Pb ages and Hf isotope characteristics and their geological significance of tuff in Wulalike Formation in the Northwestern Ordos Basin. Geological Review, 63(5), 1309–1327 (in Chinese with English abstract).

Wu, C., Zuza, A. V., Yin, A., Liu, C., Reith, R. C., Zhang, J., et al. (2017b). Geochronology and geochemistry of Neoproterozoic granitoids in the central Qilian Shan of northern Tibet: Reconstructing the amalgamation processes and tectonic history of Asia. Lithosphere, 9(4), 609–636. https://doi.org/10.1130/l640.1

Wu, D. X., Zhou, J. G., Wu, X. N., Ding, Z. C., Yu, Z., Wang, S. Y., Li, W. L., Wang, S. M. (2018). Lithofacies and palaeogeography of the Early-Middle Ordovician in the Western Ordos Basin. Geological Journal of China Universities, 24, 747–760. (in Chinese with English abstract).

Wu, C., Zuza, A. V., Yin, A., Chen, X., Haproff, P. J., Li, J., et al. (2021a). Punctuated orogeny during the assembly of Asia: Tectonostratigraphic evolution of the North China craton and the Qilian Shan from the Paleoproterozoic to early Paleozoic. Tectonics, 40, e2020TC006503. https://doi.org/10.1029/2020TC006503

Wu, P., Wu, Y. B., Zhou, G. Y., Zhang, W. X., & He, Y. (2021b). Geochronology, geochemistry, and isotope compositions of "Grenvillian" S-type granites in the North Qinling unit, central China: Petrogenesis and tectonic significance. Precambrian Research, 360, 106247. https://doi.org/10.1016/j.precamres.2021.106247

Xia, L. Q., Xia, Z. C., & Xu, X. Y. (2003). Magmagenesis in the Ordovician in back basins of the northern Qilian Mountains, China. Geological Society of America Bulletin, 115(12), 1510–1522. https://doi.org/10.1130/B25269.1

Xia, X. H., & Song, S. G. (2010). Forming age and tectono-petrogenesis of the Jiugequan ophiolite in the North Qilian Mountain, NW China. Chinese Science Bulletin, 55, 1899–1907 (in Chinese with English abstract).

Xia, L. Q., Xia, Z. C., Xu, X. Y., Li, X. M., Ma, Z. P. (2012). Mid-Late Neoproterozoic rift-related volcanic rocks in China: Geological records of rifting and break-up of Rodinia. Geoscience Frontiers, 3, 375–399. https://doi.org/10.1016/j.gsf.2011.10.004

Xia, L. Q., Li, X. M., Yu, J. Y., Wang, G. Q. (2016). Mid-Late Neoproterozoic to early Paleozoic volcanism and tectonic evolution of the Qilianshan, NW China. Geology Research Journal, 9–12, 1–41.

Xiao, X. C., Chen, G. M., & Zhu, Z. Z. (1978). A preliminary study on the tectonics ancient ophiolites in the Qilian Mountain, northwest China. Acta Geological Sinica, 4, 9-295 (in Chinese with English abstract).

1041 Xiao, X. C., Tang, Y. Q., & Gao, Y. L. (1986). Re-exposition on plate tectonics of the Qinghai-Xizang
1042 Plateau (in Chinese). Bulletin of Chinese Academy of Geological Sciences, 14, 7–19 (in Chinese with
1043 English abstract).
1044 Xiao, W. J., Windley, B. F., Hao, J., & Li, J. L. (2002a). Arc-ophiolite obduction in the Western Kunlun
1045 Range (China): implications for the Palaeozoic evolution of central Asia. Journal of the Geological
1046 Society of London, 159, 517–528.
1047 Xiao, W. J., Windley, B. F., Chen, H. L., Zhang, G. C., & Li, J. L. (2002b). Carboniferous-Triassic
1048 subduction and accretion in the western Kunlun, China: implications for the collisional and
1049 accretionary tectonics of the northern Tibetan Plateau. Geology, 30(4), 295–298.
1050 https://doi.org/10.1130/0091-7613(2002)030%3C0295:CTSAAI%3E2.0.CO;2
1051 Xiao, W. J., Han, B. F., Windley, B. F., Yuan, C., Zhou, F., & Li, J. L. (2003). Multiple Accretionary
1052 Orogenesis and Episodic Growth of Continents: Insights from the Western Kunlun Range, Central
1053 Asia. International Geology Review, 45, 303-328. https://doi.org/10.2747/0020-6814.45.4.303
1054 Xiao, W. J., Windley, B. F., Liu, D. Y., Jian, P., Liu, C. Z., Yuan, C., & Sun, M. (2005). Accretionary
1055 tectonics of the western Kunlun Orogen, China: A Paleozoic-early Mesozoic, long-lived active
1056 continental margin with implications for the growth of southern Eurasia. The Journal of Geology, 113,
1057 687–705. https://doi.org/10.1086/449326
1058 Xiao, W.J., Windley, B. F., Yong, Y., Yan, Z., Yuan, C., Liu, C., & Li, J. (2009). Early Paleozoic to
1059 Devonian multiple-accretionary model for the Qilian Shan, NW China. Journal of Asian Earth
1060 Sciences, 35, 323–333. https://doi.org/10.1016/j.jseaes.2008.10.001
1061 Xiao, W. J., Windley, B. F., Sun, S., Li, J. L., Huang, B. C., Han, C. M., Yuan, C., Sun, M., & Chen, H. L.
1062 (2015). A Tale of amalgamation of three Permo-Triassic collage systems in Central Asia: oroclines,
1063 sutures, and terminal accretion. Annual Review of Earth and Planetary Sciences, 43, 477–507.
1064 https://doi.org/10.1146/annurev-earth-060614-105254
1065 Xiao, W. J., Ao, S. J., Yang, L., Han, C. M., Wan, B., Zhang, J. E., Zhang, Z. Y., Li, R., Chen, Z. Y., & Song,
1066 S. H. (2017). Anatomy of composition and nature of plate convergence: Insights for alternative
1067 thoughts for terminal India-Eurasia collision. Science China Earth Sciences, 60, 1015–1039.
1068 https://doi.org/10.1007/s11430-016-9043-3
1069 Xu, Y. J., Du, Y. S., Cawood, P. A., Guo, H., Huang, H., & An, Z. H. (2010a). Detrital Zircon Record of
1070 Continental Collision: Assembly of the Qilian Orogen, China. Sedimentary Geology, 230, 35–45.

https://doi.org/10.1016/j.sedgeo.2010.06.020

Xu, Y. J., Du, Y. S., Cawood, P. A., & Yang, J. H. (2010b). Provenance record of a foreland basin: detrital zircon U-Pb ages from Devonian strata in the North Qilian Orogenic Belt, China. Tectonophysics, 495, 337–347. https://doi.org/10.1016/j.tecto.2010.10.001

Xu, Y. J., Du, Y. S., & Yang, J. H. (2013a). Tectonic Evolution of the North Qilian Orogenic Belt from the Late Ordovician to Devonian: Evidence from Detrital Zircon Geochronology. Journal of Earth Science, 5, 31–43 (in Chinese with English abstract).

Xu, Z. Q., Yang, J. S., Li, W. C., Li, H. Q., Cai, Z. H., Yan, Z., & Ma, C. Q. (2013b). Paleo-Tethys system and accretionary orogen in the Tibet Plateau. Acta Petrologica Sinica, 29, 1847–1860 (in Chinese with English abstract).

Xu, X., Song, S., Su, L., Li, Z., Niu, Y., & Allen, M. B. (2015). The 600-580 Ma continental rift basalts in north Qilian Shan, northwest China: Links between the Qilian-Qaidam block and SE Australia, and the reconstruction of east Gondwana. Precambrian Research, 257, 47–64. https://doi.org/10.1016/j.precamres.2014.11.017

Yan, Z., Wang, Z. Q., Wang, T., Yan, Q. R., Xiao, W. J., & Li, J. L. (2006). Provenance analysis and tectonic setting of the clastic deposits of the Xicheng Basin in the Qinling orogen, central China. Journal of Sedimentary research, 76(3), 557–574. https://doi.org/10.2110/jsr.2006.046

Yan, Z., Xiao, W. J., Wang, Z. Q., Li, J. L. (2007). Integrated analyses constraining the provenance of sandstones, mudstones and conglomerates, a case study: the Laojunshan conglomerate, Qilian orogen, northwest China. Canadian Journal of Earth Sciences. 44(7), 961–986. https://doi.org/10.1139/e07-010

Yan, Z., Xiao, W. J., Windley, B. F., Wang, Z. Q., & Li, J. L. (2010). Silurian clastic sediments in the North Qilian Shan, NW China: chemical and isotopic constraints on their forearc provenance with implications for the Paleozoic evolution of the Tibetan Plateau. Sedimentary Geology, 231, 98–114. https://doi.org/10.1016/j.sedgeo.2010.09.001

Yan, Z., Guo, X., Fu, C., Aitchison, J., Wang, Z., & Li, J. (2014). Detrital heavy mineral constraints on the Triassic tectonic evolution of the West Qinling terrane, NW China: Implications for understanding subduction of the Paleotethyan Ocean. The Journal of Geology, 122(5), 591–608. https://doi.org/10.1086/677264.

Yan, Z., Aitchison, J., Fu, C. L., Guo, X. Q., Niu, M. L., Xia,W. J., Li, J. L. (2015). Hualong Complex, South Qilian terrane: U-Pb and Lu-Hf constraints on Neoproterozoic microcontinental fragments

accreted to the northern Proto-Tethyan margin. Precambrian Research. 266, 65–85, https://doi.org/10.1016/j.precamres.2015.05.001.

Yan, Z., Fu, C. L., Wang, Z. Q., Yan, Q. R., Chen, L., Chen, J. L. (2016). Late Paleozoic subduction-accretion along the southern margin of the North Qinling terrane, central China: evidence from zircon U-Pb dating and geochemistry of the Wuguan Complex. Gondwana Research. 30, 97–111.

Yan, Z., Fu, C., Aitchison, J. C., Niu, M. L., Solomon, B., & Cao, B. (2019a). Early Cambrian Muli arc-ophiolite complex: A relic of the Proto-Tethys oceanic lithosphere in the Qilian Orogen, NW China. International Journal of Earth Sciences, 108, 1147–1164. https://doi.org/10.1007 /s00531-019-01699-6.

Yan, Z., Fu, C. L., Aitchison, J. C., Buckman, S., Niu, M. L., Cao, B., Sun, Y., Guo, X. Q., Wang, Z. Q., Zhou, R. J. (2019b). Retro-foreland basin development in response to Proto-Tethyan Ocean closure, NE Tibet Plateau. Tectonics 38, 4229–4248. https://doi.org/10.1029/2019TC005560

Yan, Z., Fu, C. L., Jonathan, C. Aitchison, Zhou, R. J., Solomon, B., & Chen, L. (2021). Silurian Sedimentation in the South Qilian Belt: Arc-Continent Collision-related Deposition in the NE Tibet Plateau?. Acta Geologica Sinica (English Edition), 94(4), 901–913. https://doi.org/10.1111/1755-6724.14551

Yang, J. H., Du, Y. S., Cawood, P. A., & Xu, Y. J. (2009). Silurian Collisional Suturing onto the Southern Margin of the North China Craton: Detrital Zircon Geochronology Constraints from the Qilian Orogen. Sedimentary Geology, 220, 95–104. https://doi.org/10.1016/j.sedgeo.2009.07.001

Yang, F. (2015). Marine basin prototype of early Paleozoic in the southwestern Ordos block and its restriction on oil and gas geological conditions. Dissertation, Northwest University (in Chinese with English abstract).

Yang, H., Fu, J. H., Yuan, X. Q. (2011). Atlas of geological profiles of the western Ordos Basin. Petroleum industry press, Beijing 1–541. (in Chinese).

Yang, L., Song, S., Su, L., Niu, Y., Allen, M. B., Zhang, G., & Zhang, Y. (2019). Heterogeneous oceanic arc volcanic rocks in the South Qilian Accretionary Belt (Qilian Orogen, NW China). Journal of Petrology, 60, 85–116. https://doi.org/10.1093/petrology/egy107

Yin, A., & Harrison, T. M. (2000). Geologic evolution of the Himalayan-Tibetan orogen. Annual Review of Earth and Planetary Sciences, 28, 211–280. https://doi.org/10.1146/annurev.earth.28.1.211

Yin, A., Dang, Y. Q., Wang, L. C., Jiang, W. M., Zhou, S. P., Chen, X. H., Gehrels, G. E., & McRivette, M. W. (2008). Cenozoic tectonic evolution of Qaidam Basin and its surrounding regions (part 1): The southern Qilian Shan-Nan Shan thrust belt and northern Qaidam Basin. Geological Society of America Bulletin, 120, 813–846. https://doi.org/10.1130/B26180.1

Yin, C. Q., Zhao, G. C., Sun, M., Xia, X. P., Wei, C. J., & Leung, W. H. (2009). LA-ICP-MS U-Pb zircon ages of the Qianlishan Complex: constrains on the evolution of the Khondalite Belt in the Western Block of the North China Craton. Precambrian Research, 174, 78–94. https://doi.org/10.1016/j.precamres.2009.06.008

Yin, C. Q., Zhao, G. C., Guo, J. H., Sun, M., Xia, X. P., Zhou, X. W., & Liu, C. H. (2011). U-Pb and Hf isotopic study of zircons of the Helanshan Complex: constrains on the evolution of the Khondalite Belt in the Western Block of the North China Craton. Lithos, 122, 25–38. https://doi.org/10.1016/j.lithos.2010.11.010

Yong, Y., Xiao, W. J., Yuan, C., Li, J. L., Yan, Z., & Mao, Q. G. (2008). LA-ICPMS zircon U-Pb ages of granitic plutons from the eastern sector of the central Qilian and their geologic implication. Xinjiang Geology, 26, 62–70 (in Chinese with English abstract).

Yu, S. Y., Zhang, J. X., Real, P. G. D., Zhao, X. L., Hou, K. J., Gong, J. H., & Li, Y. S. (2013). The Grenvillian orogeny in the Altun-Qilian-North Qaidam mountain belts of northern Tibet Plateau: Constraints from geochemical and zircon U-Pb age and Hf isotopic study of magmatic rocks. Journal of Asian Earth Sciences, 73, 372–395. https://doi.org/10.1016/j.jseaes.2013.04.042

Yu, S. Y., Peng, Y. B., Zhang, J. X., Li, S. Z., Santosh, M., Li, Y. S., Liu, Y. J., Gao, X. Y., Ji, W. T., Lv, P., Li, C. L., Jiang, X. Z., Qi, L. L., Xie, W. M., & Xu, L. J. (2021). Tectono-thermal evolution of the Qilian orogenic system: Tracing the subduction, accretion and closure of the Proto-Tethys Ocean. Earth-Science Review, 215, 103547. https://doi.org/10.1016/j.earscirev.2021.103547

Yuan, W., & Yang, Z. Y. (2015). The Alashan terrane was not part of North China by the late Devonian: evidence from detrital zircon U-Pb geochronology and Hf isotopes. Gondwana Research, 27, 1270-1282. https://doi.org/10.1016/j.gr.2013.12.009

Zhang, J. X., & Gong, J. H. (2018). Revisiting the nature and affinity of the Alxa Block. Acta Petrologica Sinica, 34, 940–962 (in Chinese with English abstract).

Zhang, J. X., Zhang, Z. M., Xu, Z. Q., Yang, J. S., & Cui, J. W. (2001). Petrology and geochronology of eclogites from the western segment of the Altyn Tagh, Northwestern China. Lithos, 56, 187–206.

https://doi.org/10.1016/S0024-4937(00)00052-9

Zhang, J. X., Meng, F. C., and Wan, Y. S. (2007). A cold Early Palaeozoic subduction zone in the North Qilian Mountains, NW China: petrological and U-Pb geochronological constraints. Journal of Metamorphic Geology, 25, 285–304. https://doi.org/10.1111/j.1525-1314.2006.00689.x

Zhang, J., Li, J. Y., Liu, J. F., & Feng, Q. W. (2011). Detrital zircon U-Pb ages of Middle Ordovician flysch sandstones in the western Ordos margin: New constraints on their provenances, and tectonic implications. Journal of Asian Earth Sciences, 42, 1030–1047. https://doi.org/10.1016/j.jseaes.2011.03.009

Zhang, J. X., Gong, J. H., Yu, S. Y., Li, H. K., & Hou, K. J. (2013). Neoarchean-Paleoproterozoic multiple tectonothermal events in the western Alxa block, North China Craton and their geological implication: Evidence from zircon U-Pb ages and Hf isotopic composition. Precambrian Research, 235, 36–57. https://doi.org/10.1016/j.precamres.2013.05.002

Zhang, J. X., Yu, S. Y., Li, Y. S., Yu, X. X., Lin, Y. H., & Mao, X. H. (2015a). Subduction, accretion and closure of Proto-Tethyan Ocean: Early Paleozoic accretion/collision orogeny in the Altun-Qaidam-North Qilian orogenic system. Acta Petrologica Sinica, 31, 3531–3554 (in Chinese with English abstract).

Zhang, J., Zhang, Y. P., Xiao, W. X., Wang, Y. N., & Zhang, B. H. (2015b). Linking the Alxa Terrane to the eastern Gondwana during the Early Paleozoic: constraints from detrital zircon U-Pb ages and Cambrian sedimentary records. Gondwana Research, 28, 1168–1182. https://doi.org/10.1016/j.gr.2014.09.012

Zhang, J., Zhang, B. H., & Zhao, H. (2016). Timing of amalgamation of the Alxa Block and the North China Block: constraints based on detrital zircon U-Pb ages and sedimentologic and structural evidence. Tectonophysics, 668–669, 65–81. https://doi.org/10.1016/j.tecto.2015.12.006

Zhang, Y. P., Zhang, J., Chen, X. H., Wang, Y. N., Zhao, H., Nie, F. J., & Zhang, B. H. (2017). Late Palaeozoic tectonic setting of the southern Alxa Block, NW China: Constrained by age and composition of diabase. International Geology Review, 59, 1028–1046. https://doi.org/10.1080/00206814.2016.1253036

Zhang, J. X., Mattinson, C., Yu, S. Y., Li, Y. S., Yu, X. X., Mao, X. H., Lu, Z. L., & Peng, Y. B. (2018). Two contrasting accretion v. collision orogenies: Insights from early Paleozoic polyphase metamorphism in the Altun-Qilian-North Qaidam orogenic system, NW China, in Zhang, L.F., Zhang, Z., Schertl, H.P.,

& Wei, C.J. (Eds.), HP-UHP Metamorphism and Tectonic Evolution of Orogenic Belts (Vol. 471, pp. 153–181). Geological Society, London, Special Publication 474.https://doi.org/10.1144/SP474.8

Zhang, Y. D., Zhan, R. B., Zhen, Y. Y., Wang, Z. H., Yuan, W. W., Fang, X., Ma, X., & Zhang, J. P. (2019a). Ordovician integrative stratigraphy and timescale of China. Science China Earth Sciences, 62, 61–88. https://doi.org/10.1007/s11430-017-9279-0

Zhang, B. H., Zhang, J., Zhao, H., Nie, F. J., Wang, Y. N., & Zhang, Y. P. (2019b). Tectonic evolution of the western Ordos Basin during the Palaeozoic-Mesozoic time as constrained by detrital zircon ages. International Geology Review, 61, 461–480. https://doi.org/10.1080/00206814.2018.1431963

Zhao, G. C., & Cawood, P. A. (2012). Precambrian geology of China. Precambrian Research, 222–223, 13–54. https://doi.org/10.1016/j.precamres.2012.09.017

Zhao, G. C., Sun, M., & Wilde, S. A. (2002). Major tectonic units of the North China Craton and their Paleoproterozoic assembly. Science China-Earth Sciences, 32, 538–549 (in Chinese with English abstract).

Zhao, G. C., Sun, M., Wilde, S. A., & Li, S.Z. (2005). Late Archean to Paleoproterozoic evolution of the North China Craton: Key issues revisited. Precambrian Research, 136(2), 177–202. https://doi.org/10.1016/j.precamres.2004.10.002

Zhao, G. C., Cawood, P. A., Wilde, S. A., Sun, M., Zhang, J., He, Y. H., & Yin, C. Q. (2012). Amalgamation of the North China Craton: key issues and discussion. Precambrian Research, 222–223, 55–76. https://doi.org/10.1016/j.precamres.2012.09.016

Zhao, J. X., Li, F. J., Zhu, G. S., Su, Z. T., Zou, M., Wang, Y. P., & Zhou, J. L. (2014). The basic characteristics, spatial-temporal distribution, and building model of reefs in the western margin of the Ordos Basin of Ordovician. Acta Petrologica Sinica, 30, 747–756.

Zhao, G. C., Wang, Y., Huang, B., Dong, Y., Li, S., Zhang, G., & Yu, S. (2018). Geological reconstructions of the East Asian blocks: From the breakup of Rodinia to the assembly of Pangea. Earth-Science Reviews, 186, 262–286. https://doi.org/10.1016/j.earscirev.2018.10.003

Zhao, X.C., Liu, C.Y., Duan, L., Fu, C.Q., & Jin, M.Q. (2019). Two-stage magmatic events of the early Paleozoic in the eastern Hexi Corridor Belt, NW China: petrogenesis and tectonic implications. Arabian Journal of Geosciences, 12, 440. https://doi.org/10.1007/s12517-019-4605-8

Zhao, S. J., Li, S. Z., Cao, H. H., Li, X. Y., Liu, X., Yu, S. Y., & Guo, X. Y. (2020). A missing link of the Proto-Tethys Ocean between the Qinling and Qilian orogens, China: Insights from geochronology and

structural geology. Geoscience Frontiers, 11, 1495–1509. https://doi.org/10.1016/j.gsf.2020.05.009

Zhen, Y. Y., Zhang, Y. D., Wang, Z. H., & Percival, I. G. (2016). Huaiyuan Epeirogeny-Shaping Ordovician stratigraphy and sedimentation on the North China Platform. Palaeogeography, Palaeoclimatology, Palaeoecology, 448, 363-370. https://doi.org/10.1016/j.palaeo.2015.07.040

Zuza, A. V., & Yin, A. (2017). Balkatach hypothesis: A new model for the evolution of the Pacific, Tethyan, and Paleo-Asian oceanic domains. Geosphere, 13(5), 1664–1712. https://doi.org/10.1130/ges01463.1

Zuza, A. V., Wu, C., Reith, R. C., Yin, A., Li, J. H., Zhang, J. Y., et al. (2018). Tectonic evolution of the Qilian Shan: An early Paleozoic orogeny reactivated in the Cenozoic. Geological Society of America Bulletin, 130(5–6), 881–925. https://doi.org/10.1130/B31721.1

Table Caption

Supplementary Table 01. Laser ablation-inductively coupled plasma-mass spectrometry data of detrital zircons from the Cambrian and Ordovician sandstones from eastern Qilian Orogen and western North China Block.

Figure Caption

Figure 01. (a) Tectonic outline of the mainland China showing the location of the Central China Orogenic System (modified after Zhao & Cawood, 2012); (b) Geologic sketch of the North Qilian Orogen and western NCB illustrating tectonic division, major boundaries and geologic components (modified after Zhao et al., 2019); (c) Geophysical section of the Qilian Shan highlighting the deep relationships between the individual tectonic units (Xiao et al., 2009); (d) Litho-stratigraphy of the ENQAB and the WNCB.

Figure 02. Stratigraphic log of the Ordovician sequence in the WNCB. The distribution of conodonts and radiolarian nannofossils that constrains the age of individual stratigraphic units is quoted from Jing et al. (2021) and Perera & Atitchison (2021), respectively.

Figure 03. Stratigraphic profile of the lithological assemblages and interpreted sedimentary facies of the Ordovician sections/boreholes in the SWNCB (see their locations in Figure 01b).

Figure 04. Representative photographs showing stratigraphy and sedimentology of the Ordovician strata in the WNCB. Section locations are labeled in Figure 01b. Scales used in Figures 04–05 include pen (~8 cm long), geologic hammers (~35 cm long), geologists (~170 cm tall), and card (~2 cm wide). (a) Thick bedded wackestone, packstone, and grainstone of the Zhuozishan Formation at the Qinglongshan Section, with the insert photomicrograph (cross-polarized light) showing oolitic limestone from the Shibangou Section. (b) Bioclastic bearing packstone of the Zhuozishan Formation at the Qinglongshan Section with a close-up insert of Gastropoda. (c) Patch reef within thick wackestone of the Zhuozishan Formation at the Qinglongshan Section. (d) An unconformity separates the Sandbian Zhuozishan Formation and Katian Kelimoli Formation at the Qinglongshan Section. (e) Carbonate breccias within the Kelimoli Formatin at the Shibangou Section. (f) Thin bedded lime mudstone with thin tuff interlayers of the Kelimoli Formation at the Pingliang Section.

Figure 05. Representative photographs showing stratigraphy and sedimentology of the Ordovician strata in the WNCB and the ENQAB. Section locations are labeled in Figure 01b. (a) Distant view of the massive siliciclastic turbidites of the Lashizhong Formation depositionally sitting above the black shale dominated Wulalike Formation at the Xishan Section. (b) Thin bedded pelagic black graptolite-bearing shale of the Wulalike Formation at the Xishan Section. (c) Intraclastic limestone of the Wulalike Formation at the well Gutan 1. (d) Mixed carbonate and siliciclastic breccias of basal Lashizhong Formation at the Sanguan Section. (e) Siliciclastic turbidites alternating with graptolite-bearing shale of the Lashizhong Formation at the Shibangou Section. (f) Soft-sediment deformation indicating sandstone slump of the Lashizhong Formation at the Xianggen Section. (g) Massive siliciclastic turbidites of the Miboshan Formation at the Niuhoushan Section. (h) Gravity-induced mass transport deposit within sandstone turbidite of the Miboshan Formation at the Niuhoushan Section.

Figure 06. Ternary plots for the Cambrian and Ordovician sandstone modal composition data from the ENQAB and the SWNCB are shown. (A) Petrologic classification is according to Pettijohn (1975). (B–D) Provenance fields are from Dickinson & Suczek (1979). Fm.—formation; Qt—total quartz; Qm—monocrystalline quartz; Qp—polycrystalline quartz; K— K-feldspar; Pl—plagioclase;

L—lithic fragment; Qt—Qm + Qp; F—K + Pl; Lt—L + Qp. Samples of the Majiagou Formation are quoted from Sun & Dong, (2020).

Figure 07. Concordia diagrams show the results of single-grain zircon U–Pb analyses and frequency (bars) and relative probability density distribution (curves) of ages of samples from the Lashizhong Formation. Ellipses show individual analyses. Error ellipses represent 2σ uncertainties. See Supplementary Table 01 for detailed data.

Figure 08. Concordia diagrams show the results of single-grain zircon U–Pb analyses and frequency (bars) and relative probability density distribution (curves) of ages of samples from the Lashizhong and Miboshan Formations. Ellipses show individual analyses. Error ellipses represent 2σ uncertainties. See Supplementary Table 01 for detailed data.

Figure 09. Normalized relative probability density distributions (spectra) show detrital zircon U–Pb ages of the Mesoproterozoic to Middle Ordovician (a) and the Late Ordovician (b) siliciclastic rocks from the WNCB, and (c) the Late Ordovician samples from the ENQAB. (e) Cumulative probability curves of measured crystallization ages for detrital zircon grains relative to the depositional ages of samples. The base figure is modified from Cawood et al. (2012). DA, depositional age. CA, crystallization age of the youngest 5% of detrital zircons. Convergent basin (A, pink), collisional basin (B, light blue) and extensional basin (C, light green).

Figure 10. Probability density distribution (curves) of ages for: (a) Mesoproterozoic to Cambrian sandstones from the WNCB (Sun & Dong, 2020a) and Middle Ordovician Sandaokan Formation (Sun & Dong, 2020a); (b) Upper Ordovician (the Katian Lashizhong Formation) turbidites from the WNCB (this study); (c) Upper Ordovician Miboshan Formation (Zhang et al., 2016, 2017). The age spectra for the CQT basement and the NCB basement are quoted from Zhang et al. (2019c) and Wu et al. (2021b), respectively. n—number of concordant zircon U–Pb ages for each sample.

Figure 11. Schematic model showing the Late Ordovician deep-water basin-filling of the SWNCB and the Qilian Orogen (Modified from Charlotte et al., 2020). See the main text for details.

Figure 12. Theoretical block models showing the tectonic evolution of the WNCB and indicating multiple stages of evolution in paleogeography and provenance from the Early to the Late Ordovician (Modified from Xiao et al., 2017). See the main text for details.

Figure 13. Tectonic reconstructions of East Asian blocks showing closure of the Proto-Tethys Ocean (Modified from Dong et al., 2021).

Figure 01.

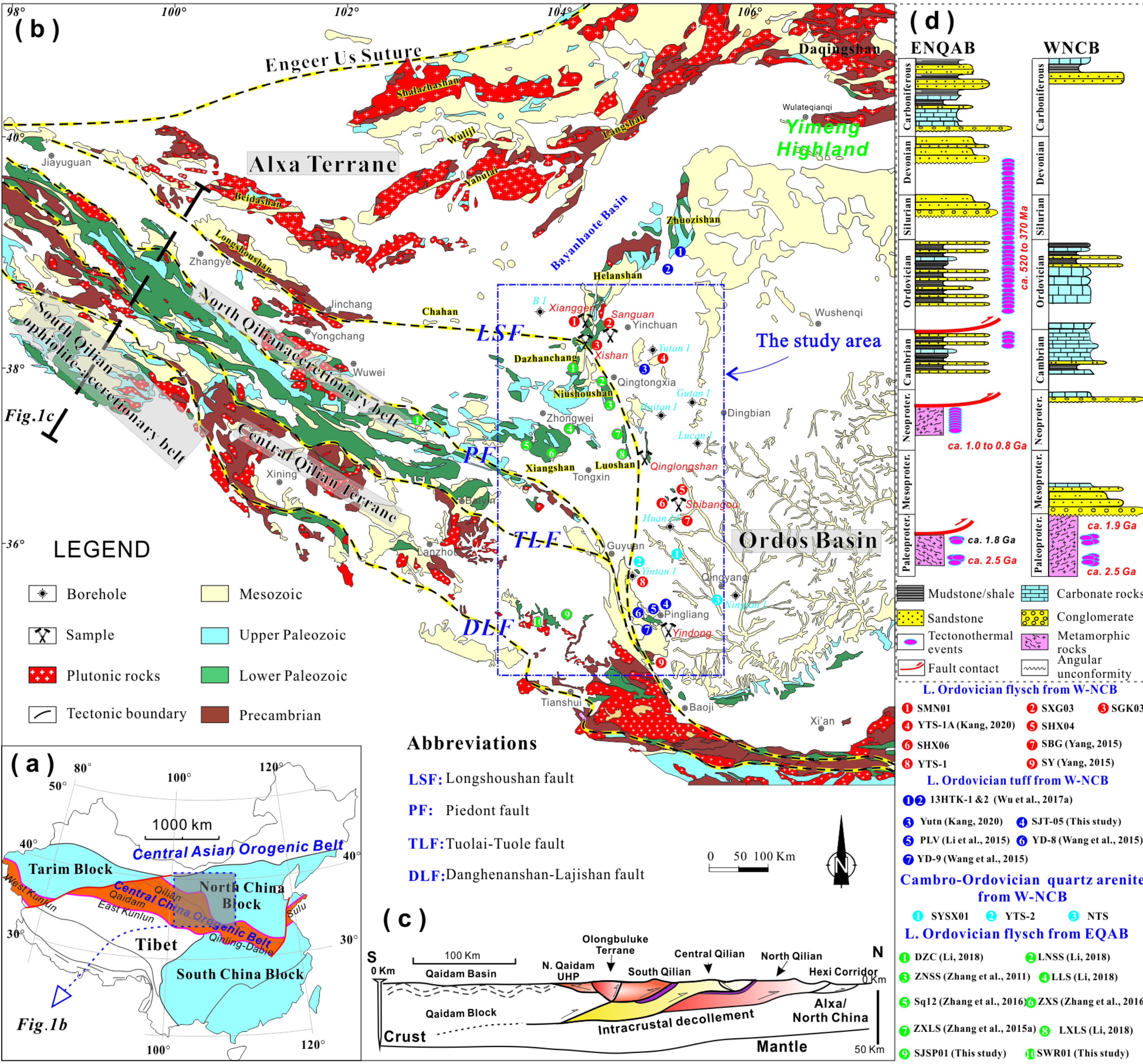
(b)
98°
100°
102°
104°
106°
Engeer Us Suture
Daqingshan
Shalazhashan
Wuliji
Langshan
Wulateqianqi
Yimeng Highland
Alxa Terrane
Jiayuguan
Beidashan
Yabulai
Longshoushan
Zhangye
Zhuozishan
Bayanhaote Basin
Helanshan
Jinchang
Chahan
B 1
Xianggen
Sanguan
Yinchuan
LSF
Wushenqi
The study area
Yongchang
North Qilian accretionary belt
South Qilian ophiolite-accretionary belt
Wuwei
Xishan
Yutan 1
Dazhanchang
Qingtongxia
Niushoushan
Gutan 1
Fig.1c
Huitan 1
Dingbian
Zhongwei
Lucan 1
PF
Central Qilian Terrane
Xiangshan
Luoshan
Tongxin
Qinglongshan
Xining
Shibangou
Baiyin
Huan 14
TLF
Ordos Basin
Guyuan
Lanzhou
Yintan 1
Qingyang
Ningtan 1
Pingliang
DLF
Yindong
Tianshui
Baoji
Xi'an
38°
36°
40°
LEGEND
Borehole
Sample
Plutonic rocks
Tectonic boundary
Mesozoic
Upper Paleozoic
Lower Paleozoic
Precambrian
Abbreviations
LSF: Longshoushan fault
PF: Piedont fault
TLF: Tuolai-Tuole fault
DLF: Danghenanshan-Lajishan fault
0 50 100 Km
N
(a)
80°
100°
120°
50°
40°
30°
1000 km
Central Asian Orogenic Belt
Tarim Block
North China Block
West Kunlun
Qilian
Qaidam
Central China Orogenic Belt
East Kunlun
Sulu
Qinling-Dabie
Tibet
South China Block
Fig.1b
(c)
S
N
0 Km
100 Km
Qaidam Basin
N. Qaidam UHP
Olongbuluke Terrane
South Qilian
Central Qilian
North Qilian
Hexi Corridor
Qaidam Block
Intracrustal decollement
Alxa/ North China
Crust
Mantle
50 Km
(d)
ENQAB
WNCB
Carboniferous
Devonian
Silurian
Ordovician
Cambrian
Neoproter.
Mesoproter.
Paleoproter.
ca. 520 to 370 Ma
ca. 1.0 to 0.8 Ga
ca. 1.8 Ga
ca. 2.5 Ga
ca. 1.9 Ga
ca. 2.5 Ga
Mudstone/shale
Carbonate rocks
Sandstone
Conglomerate
Tectonothermal events
Metamorphic rocks
Fault contact
Angular unconformity
L. Ordovician flysch from W-NCB
1 SMN01
2 SXG03
3 SGK03
4 YTS-1A (Kang, 2020)
5 SHX04
6 SHX06
7 SBG (Yang, 2015)
8 YTS-1
9 SY (Yang, 2015)
L. Ordovician tuff from W-NCB
1 2 13HTK-1 &2 (Wu et al., 2017a)
3 Yutn (Kang, 2020)
4 SJT-05 (This study)
5 PLV (Li et al., 2015)
6 YD-8 (Wang et al., 2015)
7 YD-9 (Wang et al., 2015)
Cambro-Ordovician quartz arenite from W-NCB
1 SYSX01
2 YTS-2
3 NTS
L. Ordovician flysch from EQAB
1 DZC (Li, 2018)
2 LNSS (Li, 2018)
3 ZNSS (Zhang et al., 2011)
4 LLS (Li, 2018)
5 Sq12 (Zhang et al., 2016)
6 ZXS (Zhang et al., 2016)
7 ZXLS (Zhang et al., 2015a)
8 LXLS (Li, 2018)
9 SJSP01 (This study)
10 SWR01 (This study)

Figure 02.

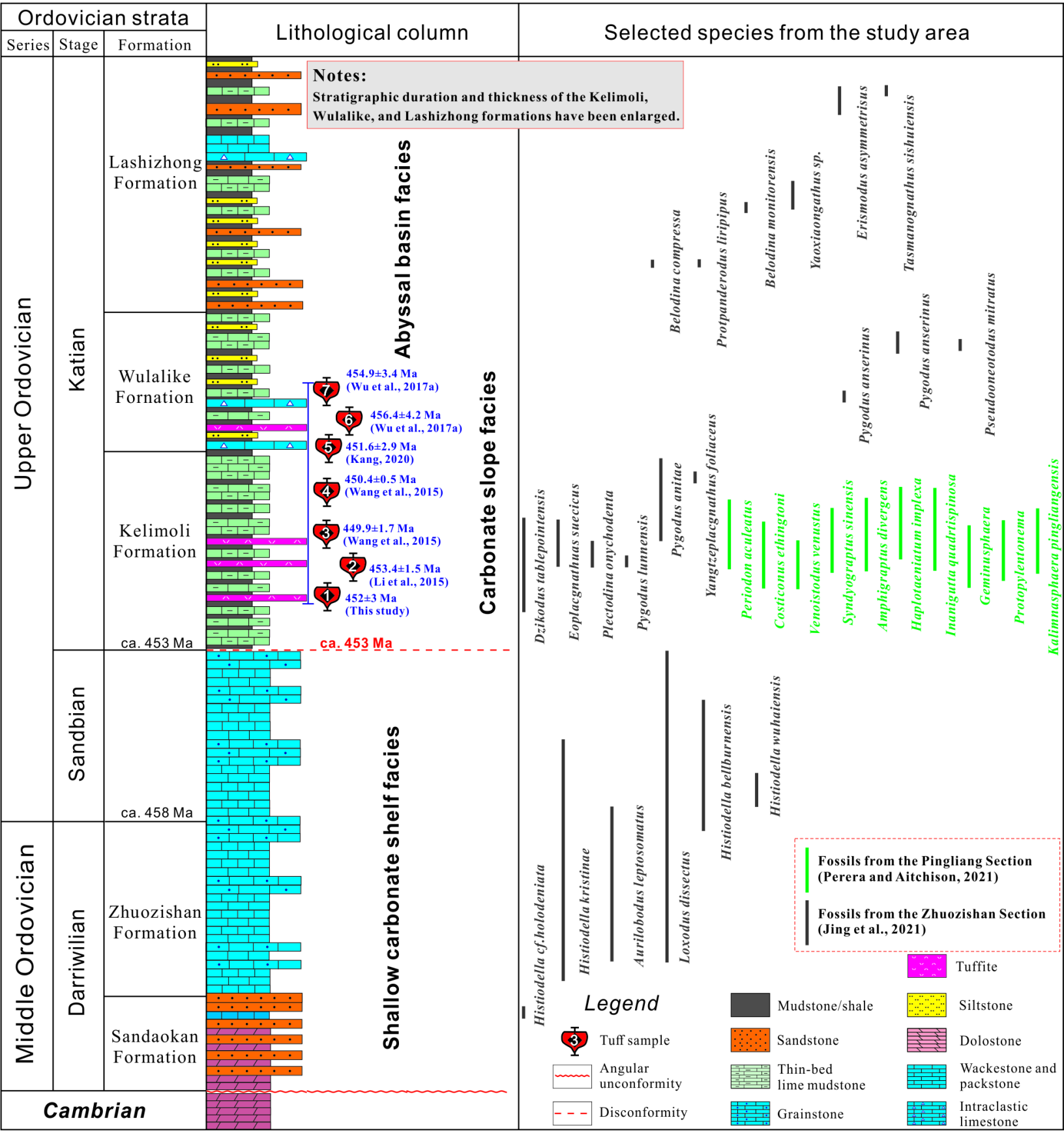
Ordovician strata
Series
Stage
Formation
Lithological column
Selected species from the study area
Upper Ordovician
Middle Ordovician
Katian
Sandbian
Darriwilian
Lashizhong Formation
Wulalike Formation
Kelimoli Formation
Zhuozishan Formation
Sandaokan Formation
Cambrian
ca. 453 Ma
ca. 458 Ma
Notes:
Stratigraphic duration and thickness of the Kelimoli, Wulalike, and Lashizhong formations have been enlarged.
Abyssal basin facies
Carbonate slope facies
Shallow carbonate shelf facies
454.9±3.4 Ma (Wu et al., 2017a)
456.4±4.2 Ma (Wu et al., 2017a)
451.6±2.9 Ma (Kang, 2020)
450.4±0.5 Ma (Wang et al., 2015)
449.9±1.7 Ma (Wang et al., 2015)
453.4±1.5 Ma (Li et al., 2015)
452±3 Ma (This study)
Dzikodus tablepointensis
Eoplacognathus suecicus
Plectodina onychodenta
Pygodus lunnensis
Pygodus anitae
Yangtzeplacgnathus foliaceus
Periodon aculeatus
Costiconus ethingtoni
Venoistodus venustus
Synduograptus sinensis
Amphigraptus divergens
Haplotaeniatum implexa
Inanigutta quadrtispinosa
Geminusphaera
Protopylentonema
Kalimnasphaera pingliangensis
Belodina compressa
Protpanderodus liripipus
Belodina monitorensis
Yaoxiaongathus sp.
Erismodus asymmetrisus
Tasmanognathus sishuiensis
Pygodus anserinus
Pygodus anserinus
Pseudooneotodus mitratus
Histiodella cf.holodeniata
Histiodella kristinae
Aurilobodus leptosomatus
Loxodus dissectus
Histiodella bellburnensis
Histiodella wuhaiensis
Fossils from the Pingliang Section (Perera and Aitchison, 2021)
Fossils from the Zhuozishan Section (Jing et al., 2021)
Legend
Tuff sample
Angular unconformity
Disconformity
Mudstone/shale
Sandstone
Thin-bed lime mudstone
Grainstone
Tuffite
Siltstone
Dolostone
Wackestone and packstone
Intraclastic limestone

Figure 03.

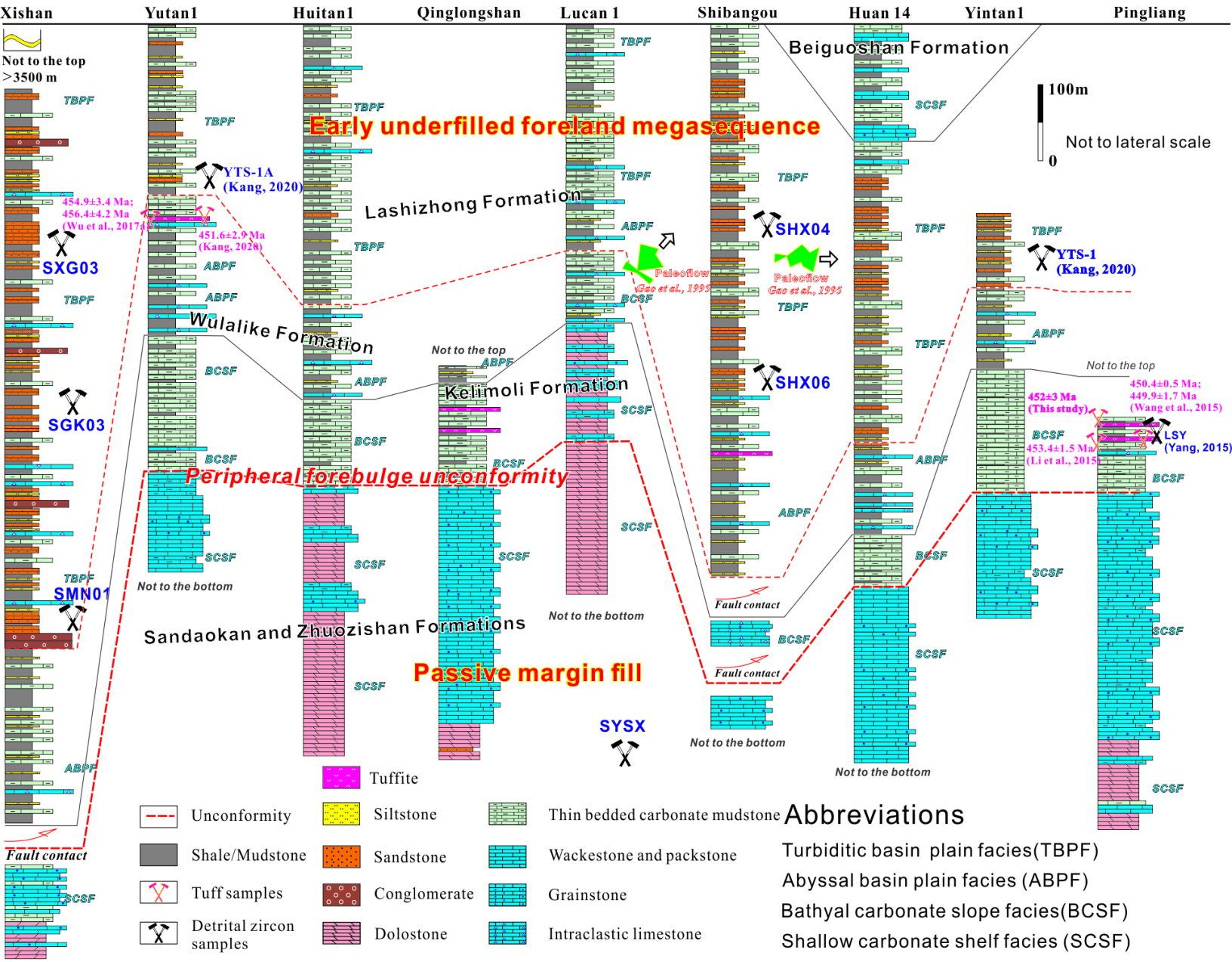
Xishan
Yutan1
Huitan1
Qinglongshan
Lucan 1
Shibangou
Huan 14
Yintan1
Pingliang
Not to the top
>3500 m
100m
Not to lateral scale
0
Beiguoshan Formation
Early underfilled foreland megasequence
Lashizhong Formation
Wulalike Formation
Kelimoli Formation
Peripheral forebulge unconformity
Sandaokan and Zhuozishan Formations
Passive margin fill
YTS-1A (Kang, 2020)
454.9±3.4 Ma; 456.4±4.2 Ma (Wu et al., 2017)
451.6±2.9 Ma (Kang, 2028)
SXG03
SGK03
SMN01
SHX04
SHX06
SYSX
YTS-1 (Kang, 2020)
452±3 Ma (This study)
453.4±1.5 Ma (Li et al., 2015)
450.4±0.5 Ma; 449.9±1.7 Ma (Wang et al., 2015)
LSY (Yang, 2015)
Paleoflow (Gao et al., 1995)
Not to the bottom
Fault contact
TBPF
ABPF
BCSF
SCSF
Tuffite
Siltstone
Thin bedded carbonate mudstone
Unconformity
Shale/Mudstone
Sandstone
Wackestone and packstone
Tuff samples
Conglomerate
Grainstone
Detrital zircon samples
Dolostone
Intraclastic limestone
Abbreviations
Turbiditic basin plain facies(TBPF)
Abyssal basin plain facies (ABPF)
Bathyal carbonate slope facies(BCSF)
Shallow carbonate shelf facies (SCSF)

Figure 04.

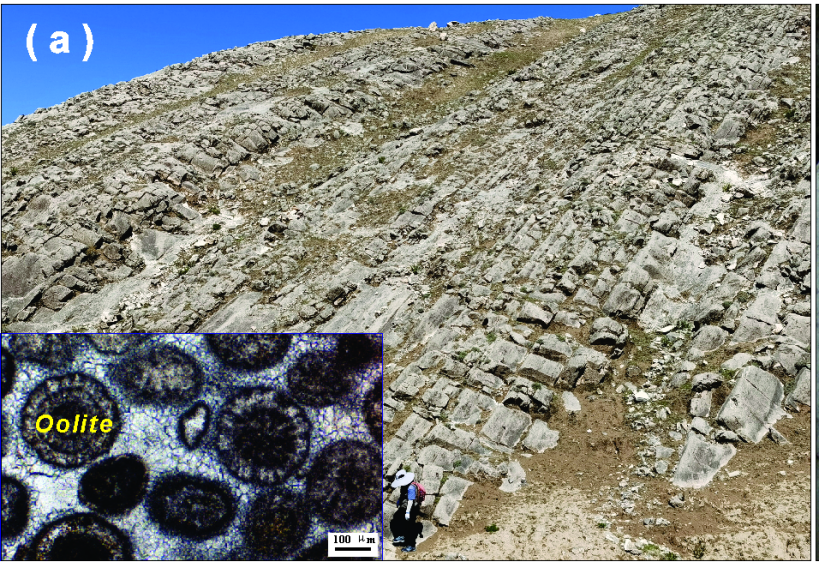
(a)
Oolite
100 μm

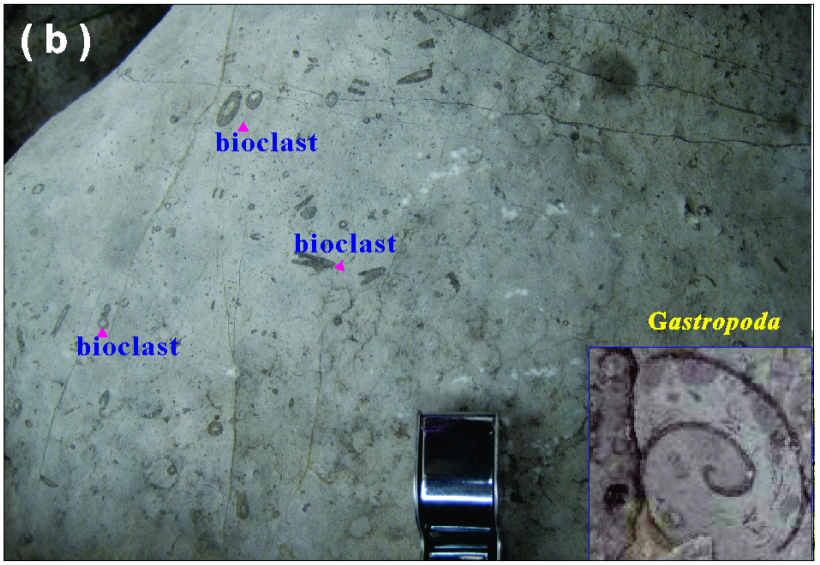
(b)
bioclast
bioclast
bioclast
Gastropoda


(c)
0
1
2
3cm

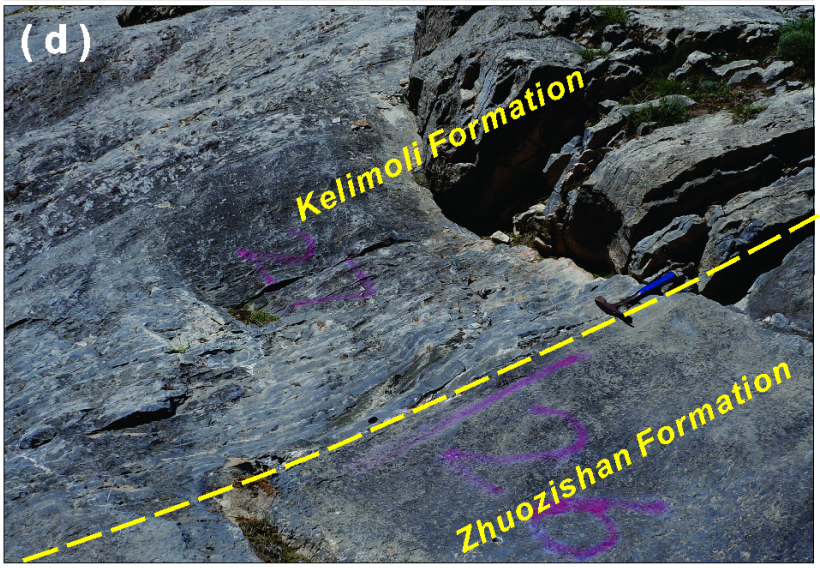
(d)
Kelimoli Formation
Zhuozishan Formation


(e)
Intraclast


(f)
Thin bedded lime mudstone
Tuff
Tuff

Figure 05.


(a)
5 cm
0
Lashizhong Formation
Wulalike Formation

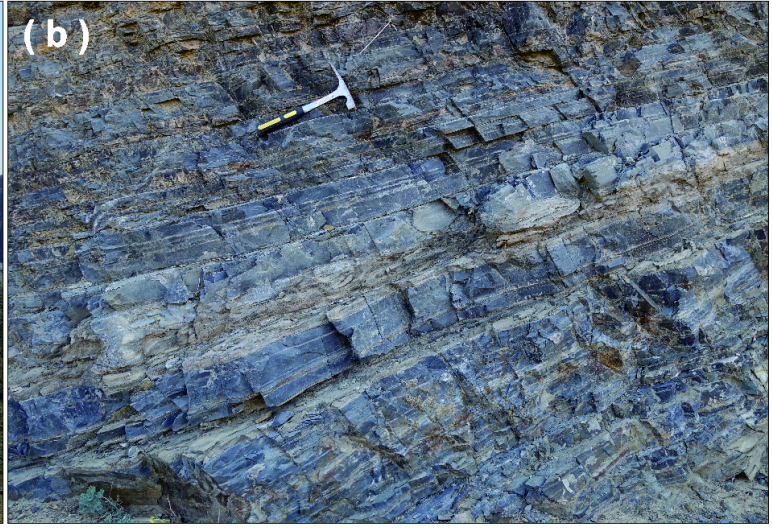
(b)

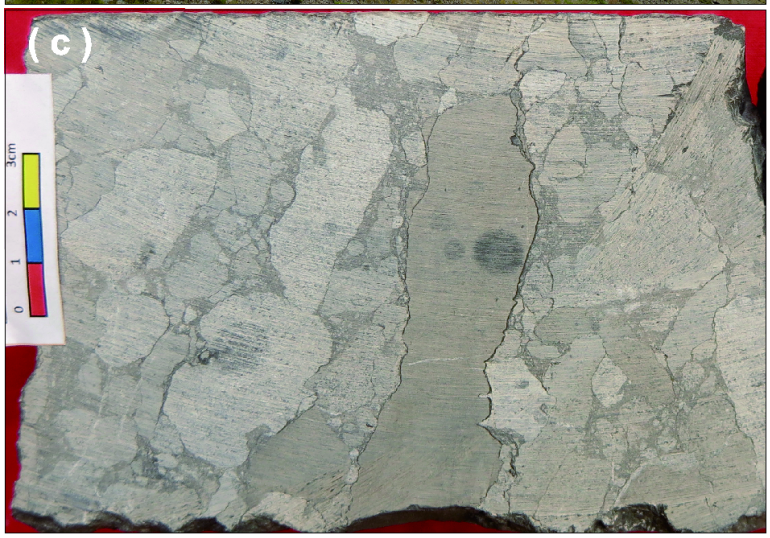
(c)
3cm
2
1
0

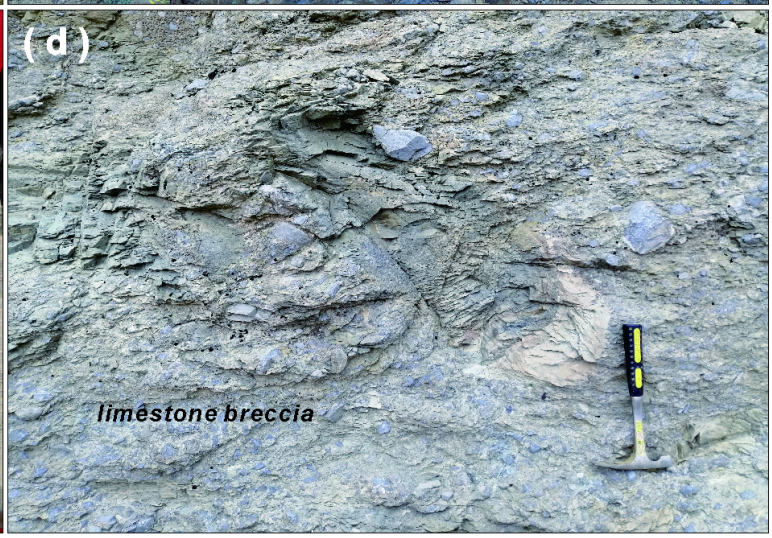
(d)
limestone breccia


(e)
normal graded coarse sandstone
flute casts on the base
erosional downcutting
shale with tabular siltstone


(f)
parallel bedding
sandstone slump


(g)


(h)
Sandstone turbidite
Gravity-induced
mass transport deposit (MTD)
Sandstone turbidite
20 cm
0

Figure 06.

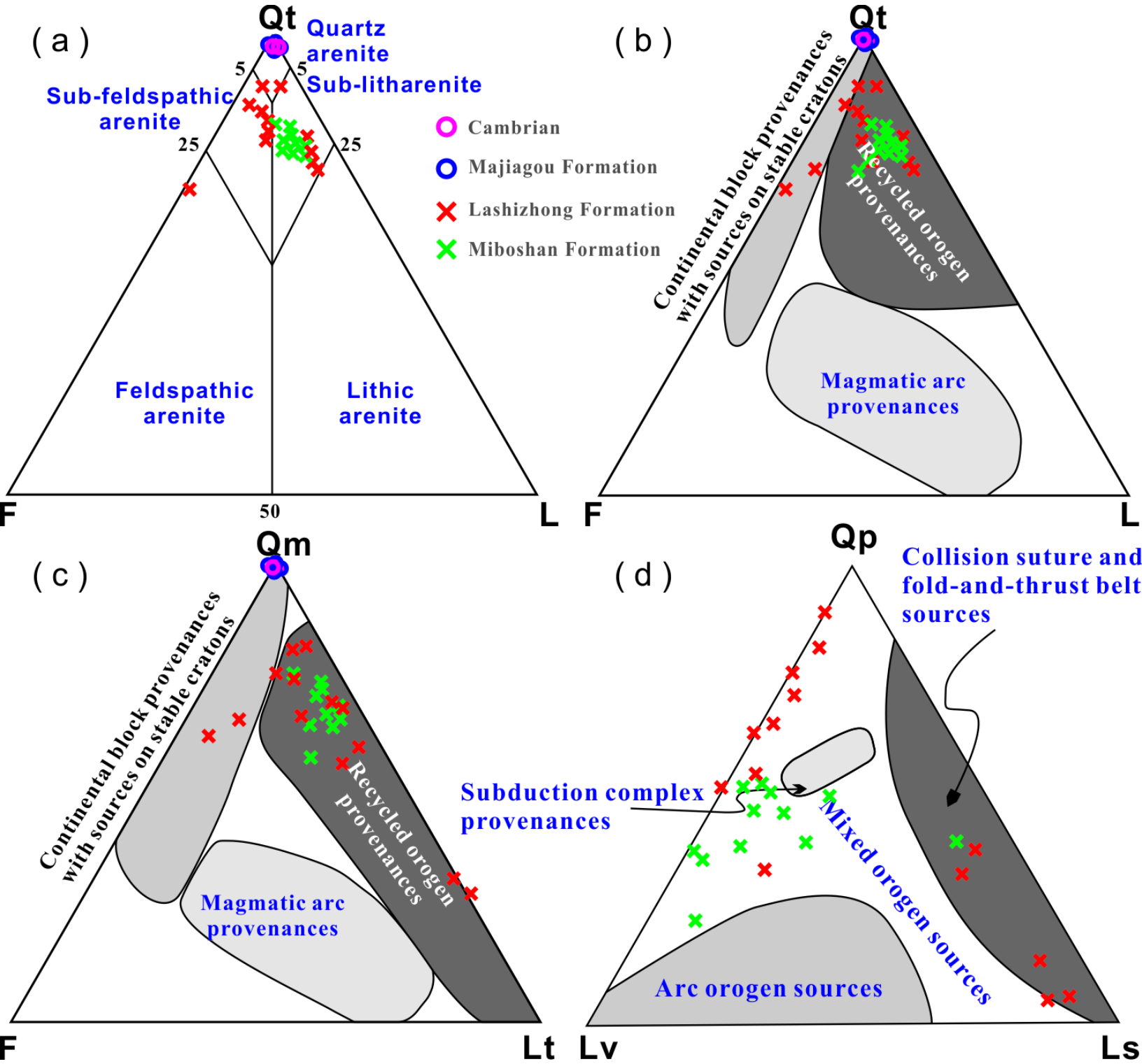
(a)
Qt
Quartz arenite
Sub-feldspathic arenite
Sub-litharenite
5
5
25
25
Cambrian
Majiagou Formation
Lashizhong Formation
Miboshan Formation
Feldspathic arenite
Lithic arenite
F
50
L
(b)
Qt
Continental block provenances with sources on stable cratons
Recycled orogen provenances
Magmatic arc provenances
F
L
(c)
Qm
Continental block provenances with sources on stable cratons
Recycled orogen provenances
Magmatic arc provenances
F
Lt
(d)
Qp
Collision suture and fold-and-thrust belt sources
Subduction complex provenances
Mixed orogen sources
Arc orogen sources
Lv
Ls

Figure 07.

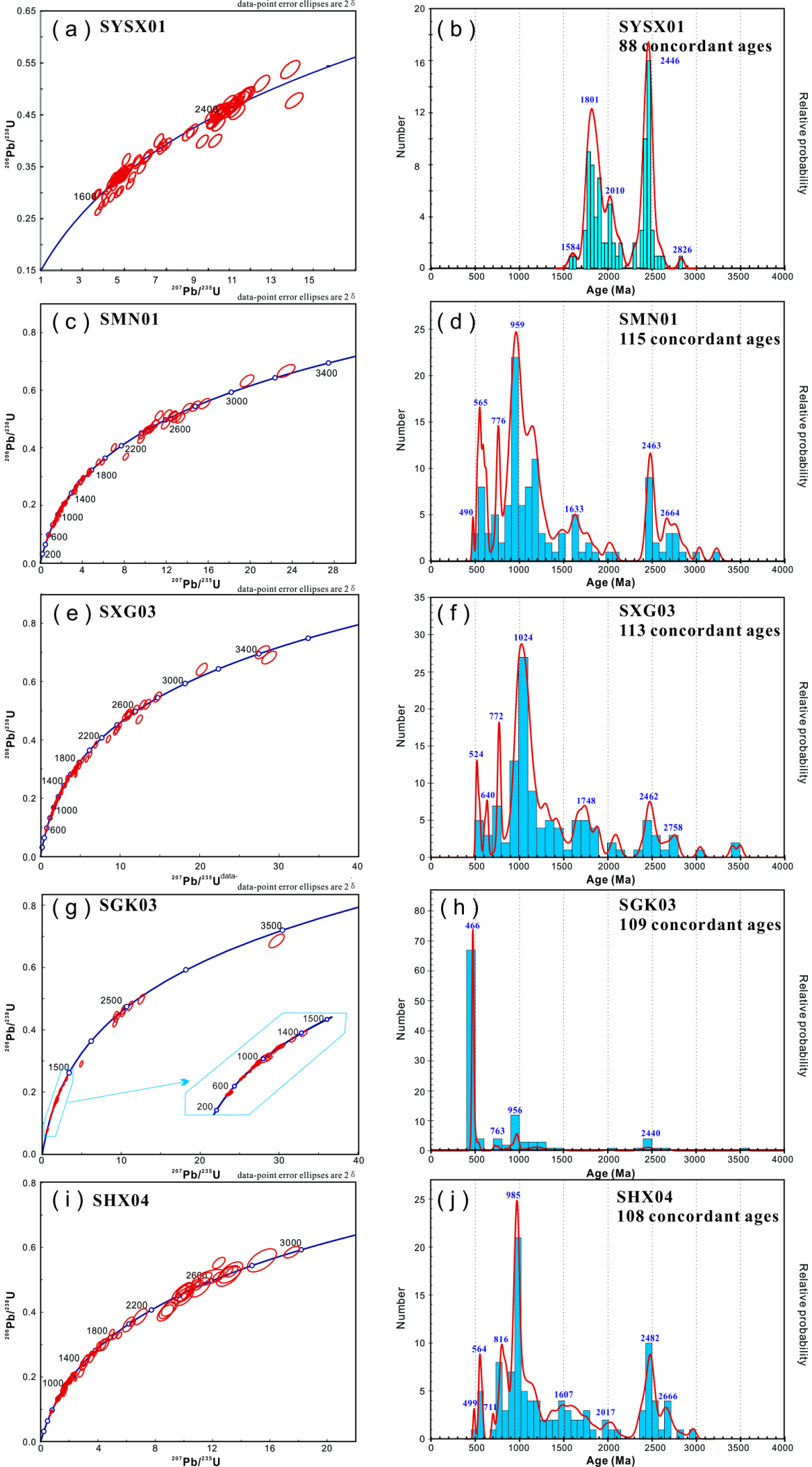
(a) SYSX01
data-point error ellipses are 2 δ
$^{206}Pb/^{238}U$
$^{207}Pb/^{235}U$
2400
1600
(b) SYSX01
88 concordant ages
2446
1801
2010
1584
2826
Number
Relative probability
Age (Ma)
(c) SMN01
data-point error ellipses are 2 δ
3400
3000
2600
2200
1800
1400
1000
600
200
(d) SMN01
115 concordant ages
959
565
776
2463
490
1633
2664
(e) SXG03
data-point error ellipses are 2 δ
(f) SXG03
113 concordant ages
1024
772
524
640
1748
2462
2758
(g) SGK03
data-point error ellipses are 2 δ
3500
2500
1500
(h) SGK03
109 concordant ages
466
956
763
2440
(i) SHX04
data-point error ellipses are 2 δ
3000
2600
2200
1800
1400
1000
(j) SHX04
108 concordant ages
985
816
564
2482
1607
499
711
2017
2666

Figure 08.

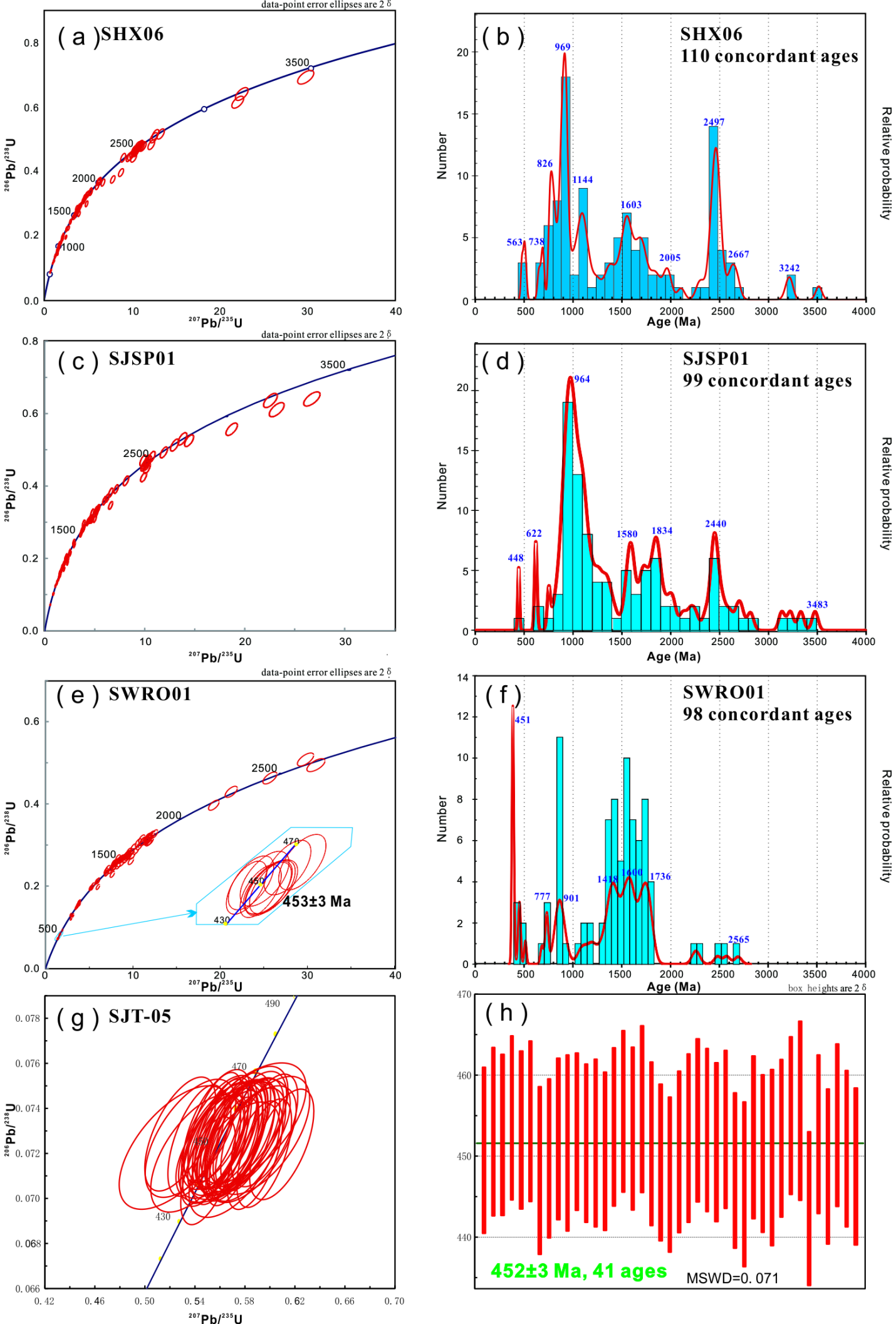
(a) SHX06
data-point error ellipses are 2 δ
3500
2500
2000
1500
1000
$^{206}Pb/^{238}U$
$^{207}Pb/^{235}U$
(b) SHX06
110 concordant ages
969
826
1144
1603
563
738
2005
2497
2667
3242
Number
Age (Ma)
Relative probability
(c) SJSP01
data-point error ellipses are 2 δ
3500
2500
1500
$^{206}Pb/^{238}U$
$^{207}Pb/^{235}U$
(d) SJSP01
99 concordant ages
964
622
448
1580
1834
2440
3483
Number
Age (Ma)
Relative probability
(e) SWRO01
data-point error ellipses are 2 δ
2500
2000
1500
500
470
450
430
453±3 Ma
$^{206}Pb/^{238}U$
$^{207}Pb/^{235}U$
(f) SWRO01
98 concordant ages
451
777
901
1415
1600
1736
2565
Number
Age (Ma)
box heights are 2 δ
Relative probability
(g) SJT-05
490
470
450
430
$^{206}Pb/^{238}U$
$^{207}Pb/^{235}U$
(h)
452±3 Ma, 41 ages
MSWD=0.071

Figure 09.

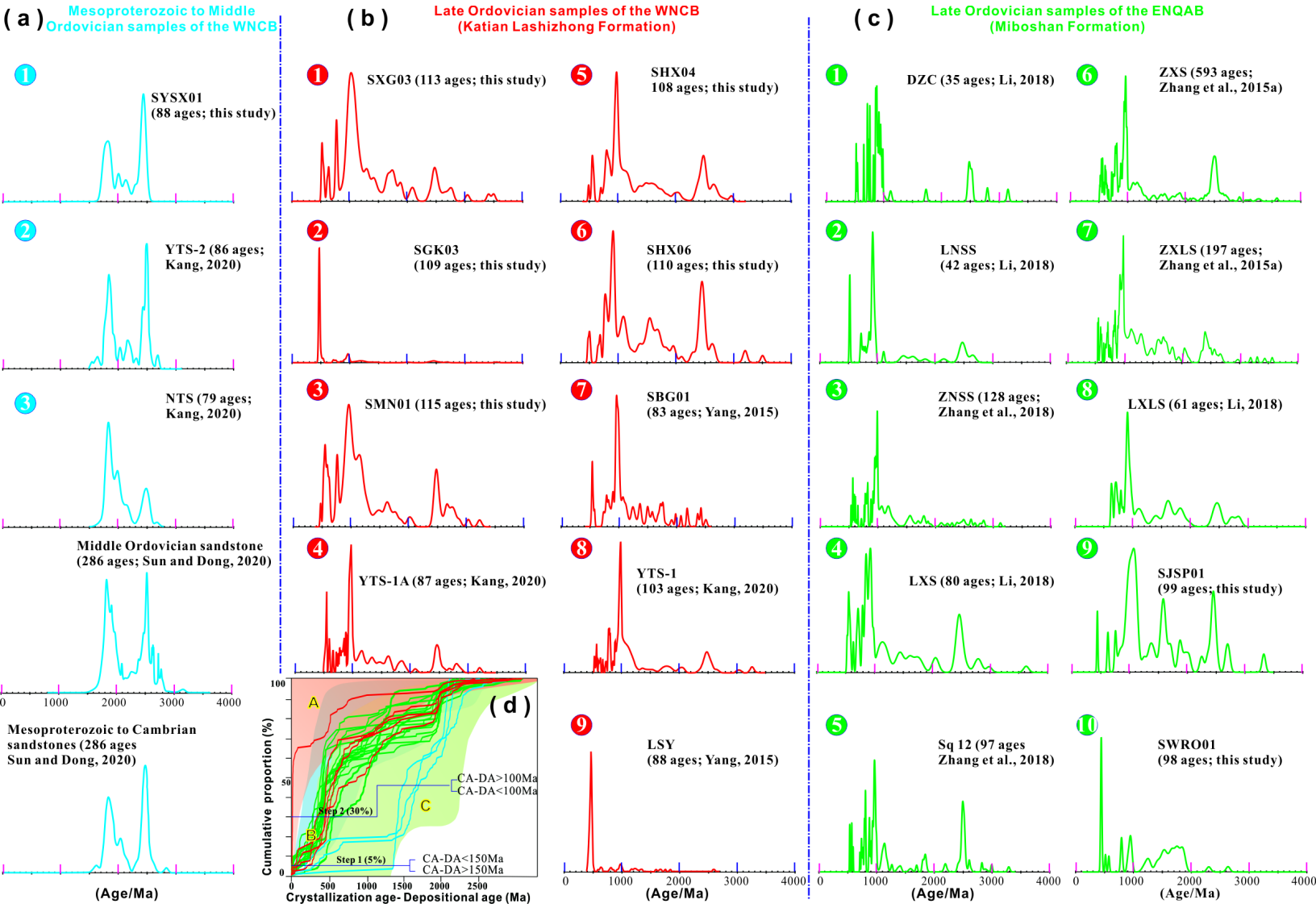
(a)
Mesoproterozoic to Middle Ordovician samples of the WNCB
1
SYSX01
(88 ages; this study)
2
YTS-2 (86 ages;
Kang, 2020)
3
NTS (79 ages;
Kang, 2020)
Middle Ordovician sandstone
(286 ages; Sun and Dong, 2020)
0
1000
2000
3000
4000
Mesoproterozoic to Cambrian
sandstones (286 ages
Sun and Dong, 2020)
(Age/Ma)
(b)
Late Ordovician samples of the WNCB
(Katian Lashizhong Formation)
1
SXG03 (113 ages; this study)
2
SGK03
(109 ages; this study)
3
SMN01 (115 ages; this study)
4
YTS-1A (87 ages; Kang, 2020)
5
SHX04
108 ages; this study)
6
SHX06
(110 ages; this study)
7
SBG01
(83 ages; Yang, 2015)
8
YTS-1
(103 ages; Kang, 2020)
9
LSY
(88 ages; Yang, 2015)
0
1000
2000
3000
4000
(Age/Ma)
(d)
A
B
C
Step 2 (30%)
Step 1 (5%)
CA-DA>100Ma
CA-DA<100Ma
CA-DA<150Ma
CA-DA>150Ma
Cumulative proportion (%)
100
50
0
0
500
1000
1500
2000
2500
Crystallization age- Depositional age (Ma)
(c)
Late Ordovician samples of the ENQAB
(Miboshan Formation)
1
DZC (35 ages; Li, 2018)
2
LNSS
(42 ages; Li, 2018)
3
ZNSS (128 ages;
Zhang et al., 2018)
4
LXS (80 ages; Li, 2018)
5
Sq 12 (97 ages
Zhang et al., 2018)
6
ZXS (593 ages;
Zhang et al., 2015a)
7
ZXLS (197 ages;
Zhang et al., 2015a)
8
LXLS (61 ages; Li, 2018)
9
SJSP01
(99 ages; this study)
10
SWRO01
(98 ages; this study)
0
1000
2000
3000
4000
(Age/Ma)

Figure 10.

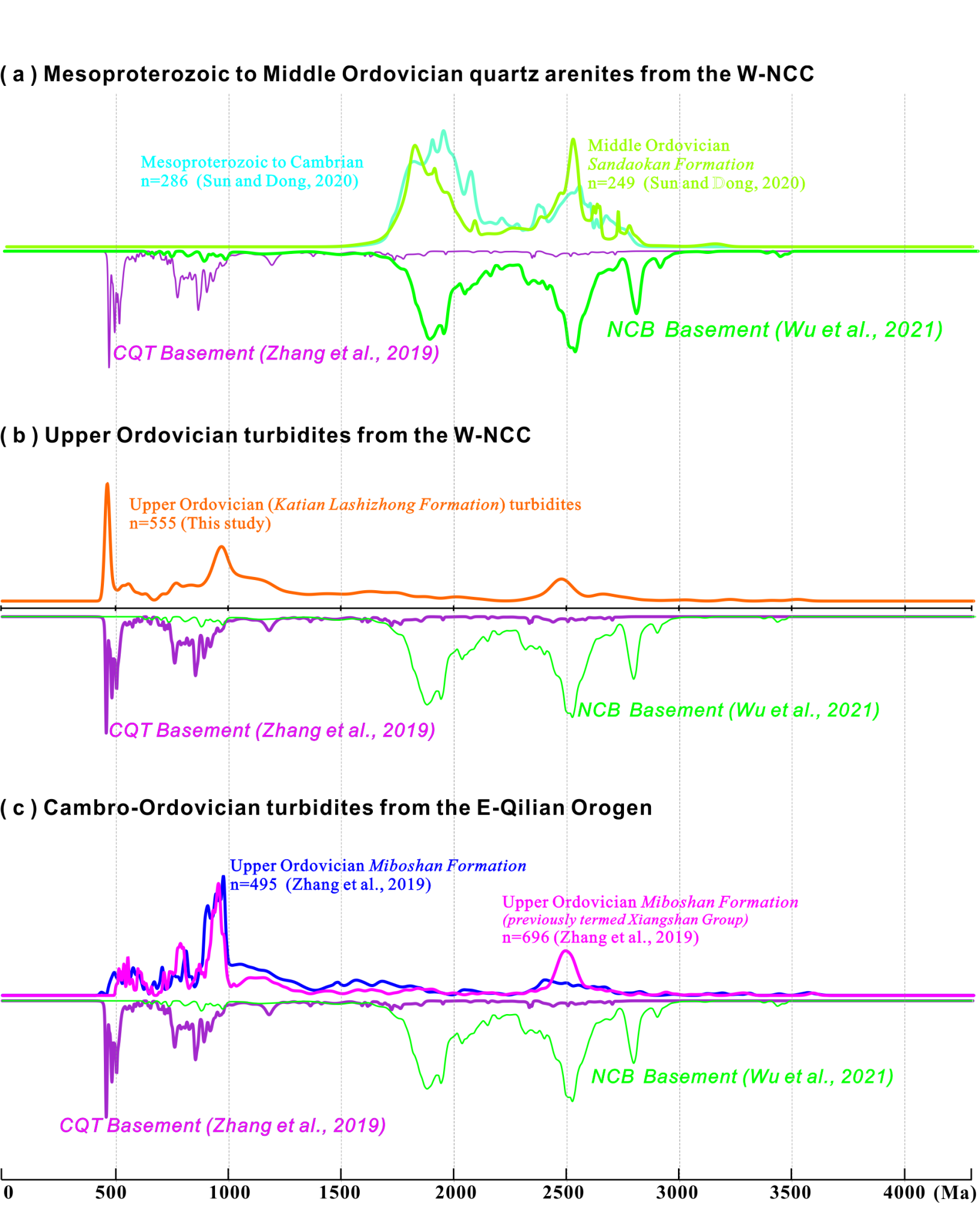
(a) Mesoproterozoic to Middle Ordovician quartz arenites from the W-NCC
Mesoproterozoic to Cambrian
n=286 (Sun and Dong, 2020)
Middle Ordovician
Sandaokan Formation
n=249 (Sun and Dong, 2020)
NCB Basement (Wu et al., 2021)
CQT Basement (Zhang et al., 2019)
(b) Upper Ordovician turbidites from the W-NCC
Upper Ordovician (Katian Lashizhong Formation) turbidites
n=555 (This study)
NCB Basement (Wu et al., 2021)
CQT Basement (Zhang et al., 2019)
(c) Cambro-Ordovician turbidites from the E-Qilian Orogen
Upper Ordovician Miboshan Formation
n=495 (Zhang et al., 2019)
Upper Ordovician Miboshan Formation
(previously termed Xiangshan Group)
n=696 (Zhang et al., 2019)
NCB Basement (Wu et al., 2021)
CQT Basement (Zhang et al., 2019)
0
500
1000
1500
2000
2500
3000
3500
4000 (Ma)

Figure 11.

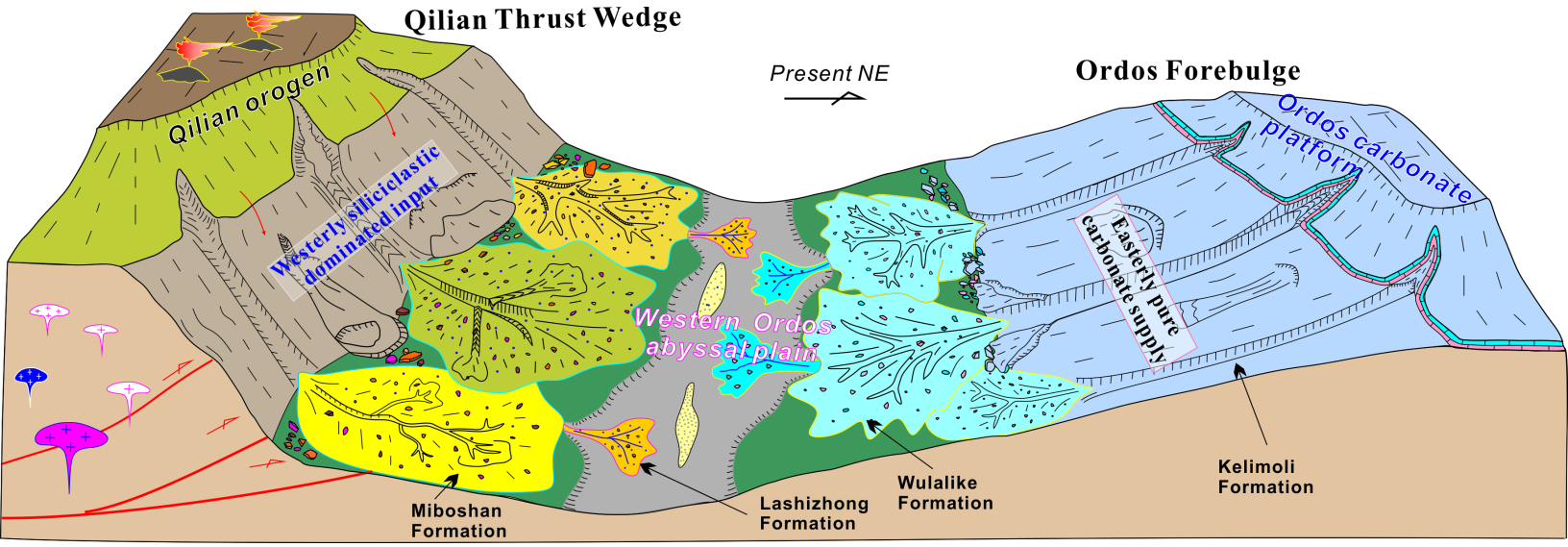
Qilian Thrust Wedge
Present NE
Ordos Forebulge
Qilian orogen
Westerly siliciclastic dominated input
Ordos carbonate platform
Easterly pure carbonate supply
Western Ordos abyssal plain
Miboshan Formation
Lashizhong Formation
Wulalike Formation
Kelimoli Formation

Figure 12.

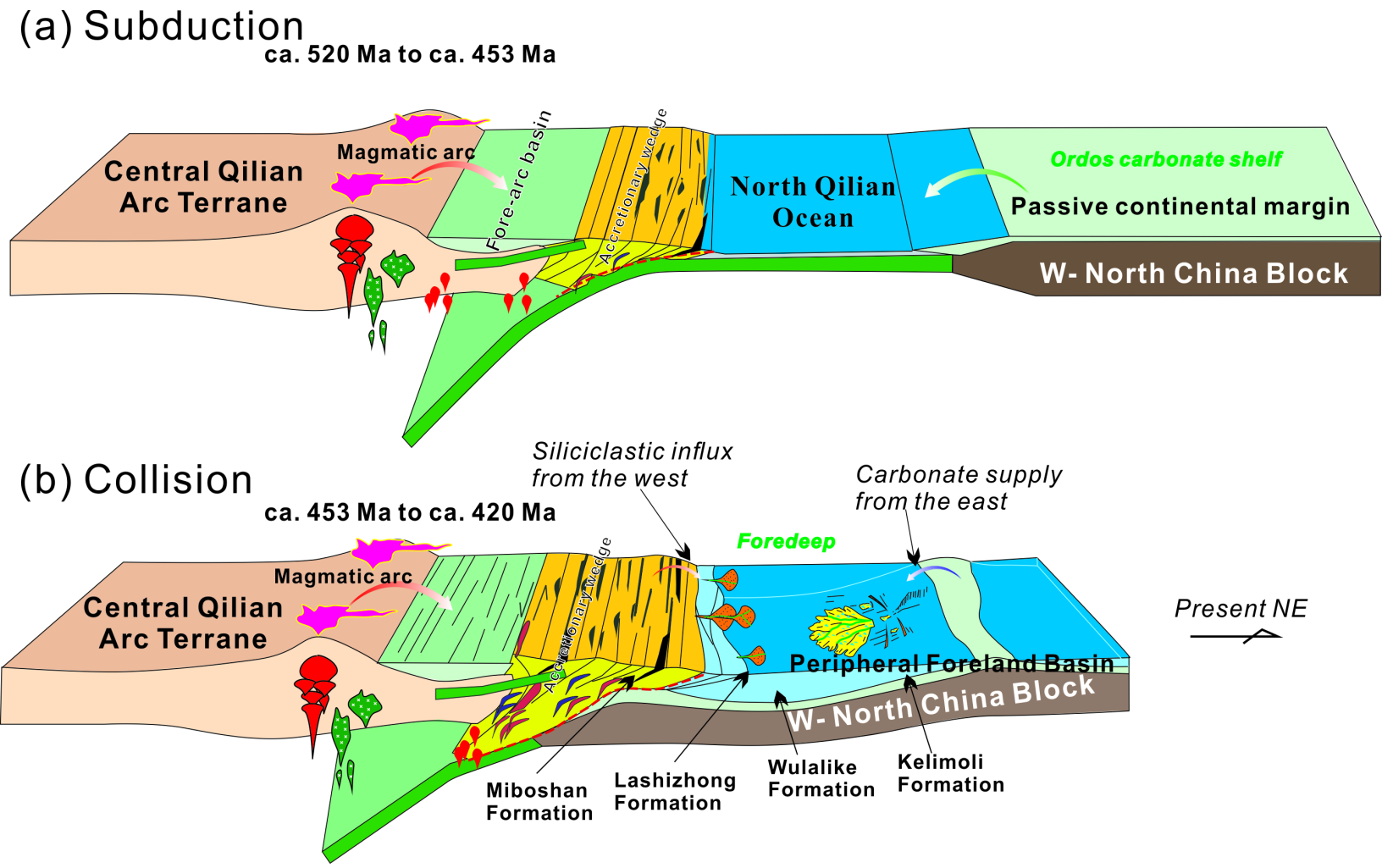
(a) Subduction
ca. 520 Ma to ca. 453 Ma
Central Qilian
Arc Terrane
Magmatic arc
Fore-arc basin
Accretionary wedge
North Qilian
Ocean
Ordos carbonate shelf
Passive continental margin
W- North China Block
(b) Collision
ca. 453 Ma to ca. 420 Ma
Siliciclastic influx
from the west
Carbonate supply
from the east
Foredeep
Magmatic arc
Central Qilian
Arc Terrane
Accretionary wedge
Peripheral Foreland Basin
W- North China Block
Present NE
Miboshan
Formation
Lashizhong
Formation
Wulalike
Formation
Kelimoli
Formation

Figure 13.

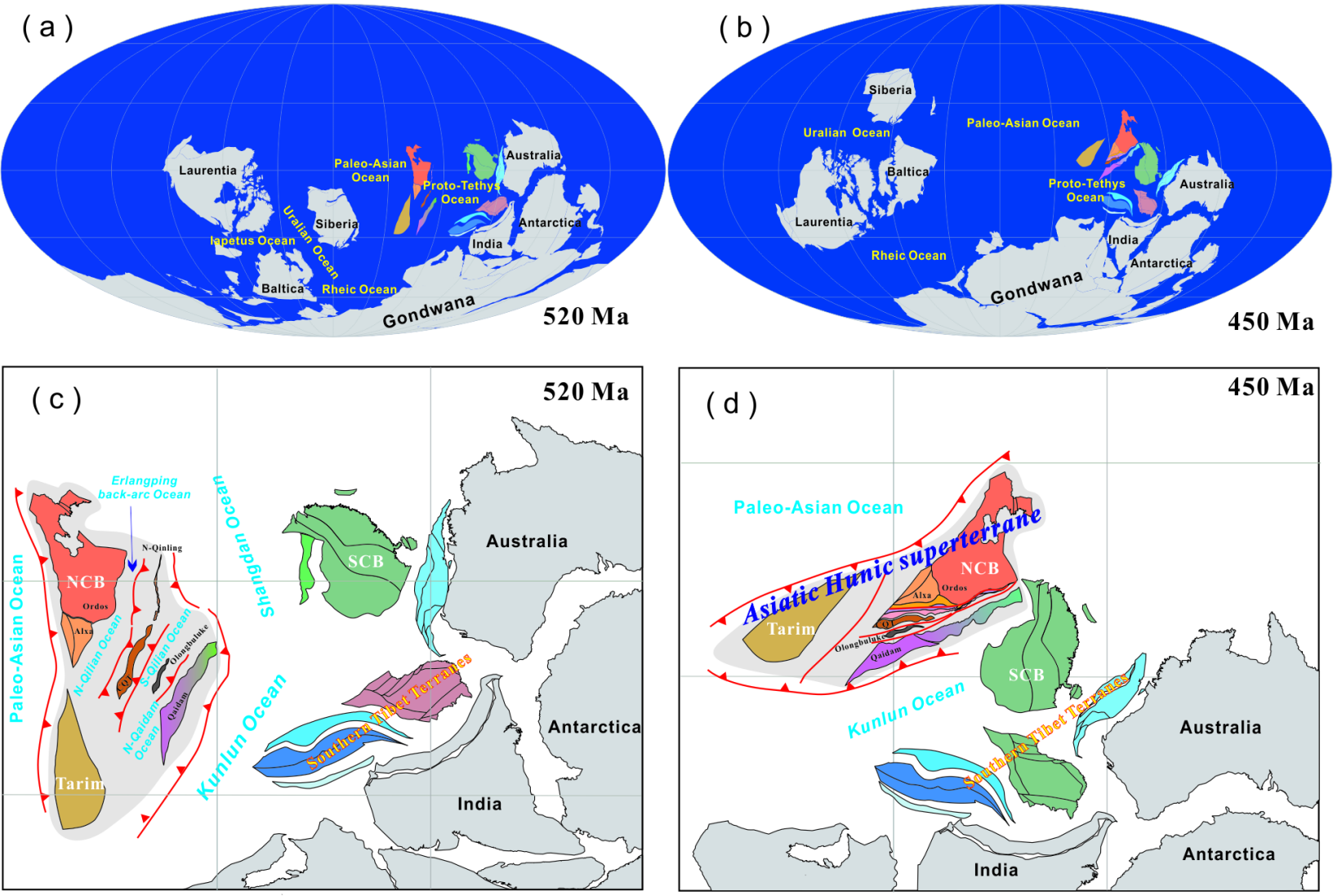
(a)
Laurentia
Paleo-Asian Ocean
Proto-Tethys Ocean
Australia
Uralian Ocean
Siberia
Antarctica
Iapetus Ocean
India
Baltica
Rheic Ocean
Gondwana
520 Ma
(b)
Siberia
Uralian Ocean
Paleo-Asian Ocean
Baltica
Proto-Tethys Ocean
Australia
Laurentia
India
Rheic Ocean
Antarctica
Gondwana
450 Ma
(c)
520 Ma
Erlangping back-arc Ocean
N-Qilian
Paleo-Asian Ocean
NCB
Ordos
Alxa
N-Qilian Ocean
S-Qilian Ocean
Oulongbuluke
Qaidam
N-Qaidam Ocean
Tarim
Shangdan Ocean
SCB
Australia
Kunlun Ocean
Southern Tibet Terranes
Antarctica
India
(d)
450 Ma
Paleo-Asian Ocean
Asiatic Hunic superterrane
NCB
Ordos
Alxa
Tarim
Oulongbuluke
Qaidam
SCB
Kunlun Ocean
Southern Tibet Terranes
Australia
India
Antarctica